J. Fluid Mech. (2008), *vol.* 600, *pp.* 105–132.
doi:10.1017/S0022112008000220 Printed in the United Kingdom

Simple analytical relations for ship bow waves

FRANCIS NOBLESSE[1], GÉRARD DELHOMMEAU[2], MICHEL GUILBAUD[3], DANE HENDRIX[1] AND CHI YANG[4]

[1]David Taylor Model Basin, NSWCCD, West Bethesda, MD, USA
[2]Laboratoire de Mécanique des Fluides (UMR CNRS n6598), École Centrale, Nantes, France
[3]Laboratoire d'Études Aérodynamiques (UMR CNRS n6609), Univ. de Poitiers, France
[4]College of Science, George Mason University, Fairfax, VA, USA

(Received 29 January 2007 and in revised form 5 December 2007)

Simple analytical relations for the bow wave generated by a ship in steady motion are given. Specifically, simple expressions that define the height of a ship bow wave, the distance between the ship stem and the crest of the bow wave, the rise of water at the stem, and the bow wave profile, explicitly and without calculations, in terms of the ship speed, draught, and waterline entrance angle, are given. Another result is a simple criterion that predicts, also directly and without calculations, when a ship in steady motion cannot generate a steady bow wave. This unsteady-flow criterion predicts that a ship with a sufficiently fine waterline, specifically with waterline entrance angle $2\alpha_E$ smaller than approximately 25°, may generate a steady bow wave at any speed. However, a ship with a fuller waterline ($25^\circ < 2\alpha_E$) can only generate a steady bow wave if the ship speed is higher than a critical speed, defined in terms of α_E by a simple relation. No alternative criterion for predicting when a ship in steady motion does not generate a steady bow wave appears to exist. A simple expression for the height of an unsteady ship bow wave is also given. In spite of their remarkable simplicity, the relations for ship bow waves obtained in the study (using only rudimentary physical and mathematical considerations) are consistent with experimental measurements for a number of hull forms having non-bulbous wedge-shaped bows with small flare angle, and with the authors' measurements and observations for a rectangular flat plate towed at a yaw angle.

1. Introduction

Free-surface flow about a ship that advances at constant speed along a straight course in calm water, i.e. a ship in steady motion, is considered. More precisely, the bow wave – arguably the most conspicuous, complex and important feature of free-surface flow about a ship – is considered. Several basic questions about ship bow waves are examined. A first, obvious, set of questions is: What is the height of the wave? What is the distance between the ship stem and the crest of the wave? What is the rise of water at a ship stem? and What is the shape of the bow wave (bow wave profile)?

A ship in steady motion is usually assumed, notably for numerical-calculation and analytical purposes, to generate a steady bow wave; but this is not always true. Common observations show that a ship in steady motion can generate an unsteady bow wave. More generally, steady motion of a body through a fluid at rest does not necessarily result in a steady flow; a classical example of unsteady flow generated by steady motion of a body in a quiescent fluid is the von Kármán vortex sheet

that can be observed (under proper conditions) behind a bluff body. Thus, another basic question is: When does a ship in steady motion generate an unsteady bow wave? A related question is: What is the height of an unsteady bow wave? No analytical or empirical relations that answer these basic questions appear to exist, to our knowledge.

A large number of well-established alternative methods have been developed to compute steady free-surface flow about a ship that advances along a straight path, with constant speed, through calm water of effectively infinite depth and lateral extent. These methods include semi-analytical theories based on various approximations (thin-ship, slender-ship, 2d+t theories), potential-flow panel (boundary integral equation) methods that rely on the use of a Green function (elementary Rankine source, or Havelock source that satisfies the radiation condition and the Michell linearized free-surface boundary condition), and computational fluid dynamics (CFD) methods that solve the Euler or RANS equations. These alternative calculation methods are reported in a huge body of literature. Only a few illustrative studies are noted here. The thin-ship theory has been widely used (e.g. Standing 1974; Noblesse & Dagan 1976). A number of alternative slender-ship and 2d+t approximations have been proposed and used (Tuck 1966; Ogilvie 1967; Chapman 1976; Noblesse 1983; Çalişal & Chan 1989; Fontaine, Faltinsen & Cointe 2000). Panel methods based on Rankine and/or Havelock sources are also widely used (e.g. Brard 1972; Dawson 1977; Jensen, Bertram & Söding 1989; Scragg & Talcott 1991; Raven 1999; Subramani, Beck & Scorpio 1999; Wyatt 2000). CFD methods are gaining popularity (e.g. Farmer, Martinelli & Jameson 1993; Hino 1997; Yang & Löhner 2002; Bulgarelli 2005; Queutey & Visonneau 2007). Flows about flat plates that pierce the free surface are considered in Chapman (1976), Maniar, Newman & Xu (1991) and Xu (1991).

These alternative calculation methods provide valuable complementary tools, which can be used to answer at least some of the basic questions raised above. In particular, existing calculation methods can be used to predict a bow wave height and profile. However, important features of free-surface flows about ships in steady motion, notably unsteady and overturning bow waves, remain difficult to model numerically and are not fully understood. In particular, we are not aware of calculation methods that can predict whether a ship in steady motion generates an unsteady bow wave. The complexities of overturning ship bow waves are well documented in the detailed experimental investigations of Dong, Katz & Huang (1997) and Roth, Mascenik & Katz (1999). These detailed experimental studies show that full numerical modelling of overturning ship bow waves involves major difficulties; nevertheless, significant progress has been reported (e.g. Tulin & Landrini 2001; Muscari & Di Mascio 2004; Landrini 2006; Wilson, Carrica & Stern 2006).

The objective of the present study and the approach adopted to achieve this objective differ markedly from the alternative objectives and methods of the literature, briefly reviewed above, on free-surface flow about a ship in steady motion. The objective of the study is to provide simple approximate analytical answers to the basic questions noted earlier. The approach that is used toward this goal relies solely on elementary fundamental considerations (dimensional analysis; asymptotic behaviour in thin-ship limit, deep or shallow draught limits; Bernoulli relation for steady flows; Lagrangian analysis based on Newton's equations for a single fluid particle; elementary sinusoidal wave) and rudimentary 'mathematical' analysis, which in fact rests entirely on simple algebraic relations. These rudimentary considerations are shown to yield useful simple relations for ship bow waves.

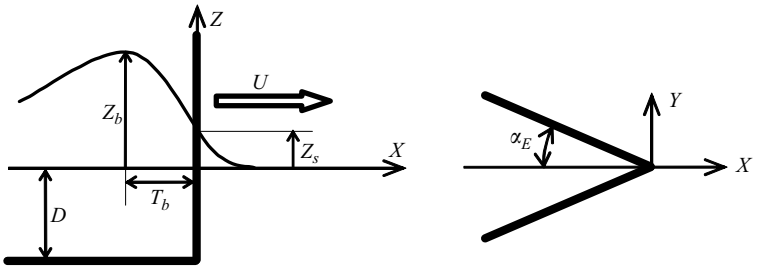

FIGURE 1. Definition sketch for the bow wave height Z_b, the rise of water Z_s at the ship stem, and the distance T_b between the bow wave crest and the ship stem, for a ship of draught D and waterline entrance angle $2\alpha_E$ that advances in calm water with speed U.

Specifically, simple expressions that define the height of a ship bow wave, the distance between the ship stem and the crest of the bow wave, the rise of water at the stem, and the bow wave profile, explicitly and without calculations, in terms of the ship speed, draught, and waterline entrance angle, are given. Another result is a simple criterion that predicts, also directly and without calculations, when a ship in steady motion cannot generate a steady bow wave. This unsteady-flow criterion predicts that a ship with a sufficiently fine waterline, specifically with waterline entrance angle $2\alpha_E$ smaller than approximately 25°, may generate a steady bow wave at any speed. However, a ship with a fuller waterline, i.e. for $25° < 2\alpha_E$, can generate a steady bow wave only if the ship speed is higher than a critical speed, which is defined in terms of α_E by a simple expression. A simple expression for the height of an unsteady ship bow wave is also given.

An important property of the simple expressions given in this study is that they provide explicit relationships between main features of a ship bow wave (wave height, location and profile; flow steadiness or unsteadiness) and basic 'design parameters' (ship speed, draught, waterline entrance angle) that define a ship. In other words, these simple expressions provide direct 'cause-and-effect' relations between basic design parameters and main bow wave characteristics. Such direct relations provide insight that is valuable for practical applications to ship design, notably at early design stages (concept and preliminary design).

2. Basic assumptions and relations

The bow wave generated by a ship hull, with a non-bulbous wedge-shaped bow of draught D and waterline entrance angle $2\alpha_E$, that advances at constant speed U in calm water is considered here. The bow flare angle γ is presumed small, and its effect on the bow wave profile is neglected. Effects of viscosity and surface tension are also ignored. However, no linearization assumption is made.

A Galilean system of coordinates (X, Y, Z) attached to the advancing ship is considered. The X- axis lies along the ship path and points toward the bow, and the Z- axis is vertical and points upward with the mean free surface taken as the plane $Z = 0$, as shown in figure 1. The velocity of the total flow (flow due to the ship + uniform stream opposing the forward speed of the ship) is $(V_x - U, V_y, V_z)$ where (V_x, V_y, V_z) is the flow due to the ship. The Froude number,

$$F_D = U/\sqrt{gD}, \tag{2.1}$$

based on the ship draught D is used, instead of the usual Froude number F based on the ship length (not relevant for the bow wave). Non-dimensional coordinates (x, y, z) and flow velocities (v_x, v_y, v_z) are defined as

$$(x, y, z) = (X, Y, Z)\, g/U^2, \qquad (v_x, v_y, v_z) = (V_x, V_y, V_z)/U, \tag{2.2}$$

where g is the acceleration due to gravity.

The steady-flow Bernoulli relation,

$$P/\rho + gZ + \left[(V_x - U)^2 + V_y^2 + V_z^2\right]/2 = P_0/\rho + U^2/2,$$

applied at the free surface, where the pressure P is equal to the atmospheric pressure P_0, and (2.2) defines the magnitude q of the total flow velocity at the free surface $z = \zeta(x, y)$ as

$$q^2 \equiv (v_x - 1)^2 + v_y^2 + v_z^2 = 1 - 2\,\zeta. \tag{2.3}$$

This expression readily yields the well-known upper bound $\zeta \leqslant 1/2$ for steady free-surface flows.

3. Experimental measurements

Further on, the simple expressions obtained in the study are compared to existing experimental measurements, reported in the literature, for several ship hulls with wedge-shaped bows, and to our measurements for a rectangular flat plate.

The experimental measurements for ship hulls with wedge-shaped bows consist of the measurements – identified as Larrarte 10°, 20° or 30° hereinafter – for three strut-like hulls that have rectangular framelines and sharp-ended parabolic waterlines with entrance angles $2\alpha_E = 20°$, 40° or 60° reported in Larrarte (1994), and measurements for eight hulls with wedge-shaped bows previously considered in Noblesse *et al.* (2006). The latter measurements consist of measurements reported in Standing (1974), Ogilvie (1973), Waniewski, Brennen & Raichlen (2002) and Karion *et al.* (2003) for seven hulls with wedge-shaped bows, and measurements reported in Kajitani *et al.* (1983) and McCarthy (1985) for the Wigley hull. These measurements are identified here as Standing 5° or 10°, Ogilvie 7.5° or 15°, Karion 10° or 20°, Waniewsky 26° and Wigley. The measurements for the Wigley hull were obtained within a cooperative experiment program under the Resistance Committee of the International Towing Tank Conference. Only measurements for the Wigley hull held in fixed position (no sinkage or trim allowed) are considered here. Two sets of measurements, reported by the Ship Research Institute and the University of Tokyo, are available for the Wigley hull.

In order to extend the foregoing experimental measurements for ship hulls with wedge-shaped bows, several series of measurements were made in the towing tank of the École Centrale de Nantes (France) with a rectangular flat plate (of length 0.782 m) immersed at a draught D and towed at a speed U, yaw angle α_E, and heel angle γ (a rotation of the flat plate about the waterline that is analogous to the flare angle of a ship hull). In a first series of experiments, the flat plate was immersed at a draught $D = 0.3$ m and towed at three yaw angles $\alpha_E = 10°$, 15°, 20° and three speeds $U = 1$, 1.5, 2 m s^{-1}, which correspond to draught-based Froude numbers $F_D \approx 0.58$, 0.87, 1.17. Additional measurements were subsequently made with the plate immersed at a draught $D = 0.2$ m and towed at yaw angles $\alpha_E = 10°$, 15°, 20°, 25°, 30°, 45°, 60°, 75°, 90°, and speeds $U = 1.25$, 1.5, 1.75, 2, 2.25, 2.5 m s^{-1}, which correspond to $F_D \approx 0.89$, 1.07, 1.24, 1.43, 1.61, 1.78. For large yaw angles α_E, high speeds U were

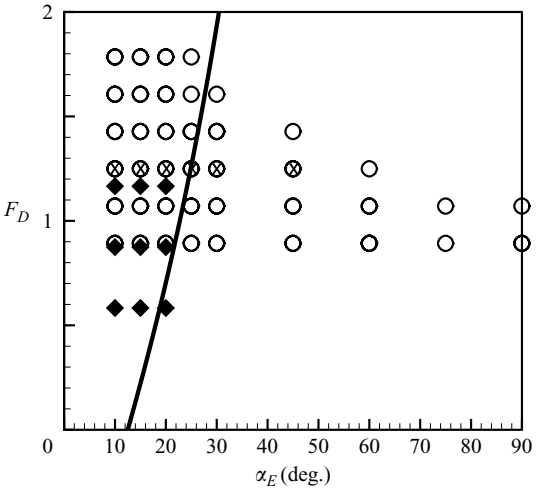

FIGURE 2. A rectangular flat plate, immersed at a draught $D = 0.2\,\mathrm{m}$ (○) or $0.3\,\mathrm{m}$ (▲), was towed at several speeds U, yaw angles α_E and heel angles γ. Wave profiles were measured for yaw angles $\alpha_E = 10°$, 15°, 20°, 25°, 30°, 45°, 60°, 75°, 90° and draught-based Froude numbers $F_D = U/\sqrt{gD} = 0.58$, 0.87, 0.89, 1.07, 1.17, 1.25, 1.43, 1.61, 1.78, as indicated in the figure, and for heel angles $\gamma = 0°$, 10°, 15°. The curve $4.4\tan\alpha_E/\cos\alpha_E - 1$ (———) separates the overturning bow wave regime (on the left-hand side of the curve) and the unsteady bow wave regime (right-hand side). ×, correspond to photographs in figure 6.

not considered because of practical concerns about excessive hydrodynamic loads on the plate. The yaw angles α_E and the Froude numbers F_D for which the wave profile along the plate was measured are indicated in figure 2. Measurements were made for three heel angles $\gamma = 0°$ (vertical plate), 10°, 15° for every value of D, U and α_E. Thus, only small heel angles γ are considered here. Figures 17, 19 and 21 show that, for the small heel angles $0° \leqslant \gamma \leqslant 15°$ considered here, wave profiles are not overly affected by γ. As illustrated in figure 6, visual observations of free-surface flows about a rectangular flat plate for the set of yaw angles α_E and Froude numbers F_D indicated in figure 2 can be divided into two basic flow regimes, for which an overturning wave or an unsteady wave is observed. The curve in figure 2, defined by (5.3), separates the overturning bow wave regime (on the left-hand side of the curve) and the unsteady bow wave regime (right-hand side).

4. Height of an overturning ship bow wave

The simple expression for the height Z_b of a ship bow wave given in Noblesse *et al.* (2006), required further on, is now briefly considered. The bow wave height Z_b is the highest water elevation, measured from the horizontal plane $Z = 0$ of the undisturbed free surface (figure 1). Simple fundamental theoretical considerations (dimensional analysis, and rudimentary asymptotic considerations in the thin-ship, shallow-draught and deep-draught limits) are used with experimental measurements in Noblesse *et al.* (2006) to express the non-dimensional bow wave height as

$$z_b \equiv \frac{Z_b g}{U^2} \approx \frac{2.2}{1 + F_D}\frac{\tan\alpha_E}{\cos\alpha_E}. \tag{4.1}$$

In the high-Froude-number-thin-ship limit $F_D \to \infty$ and $\alpha_E \to 0$, (4.1) yields $Z_b \sim 2.2\,\alpha_E\,U\sqrt{D/g}$. This approximation and the high-Froude-number approximation

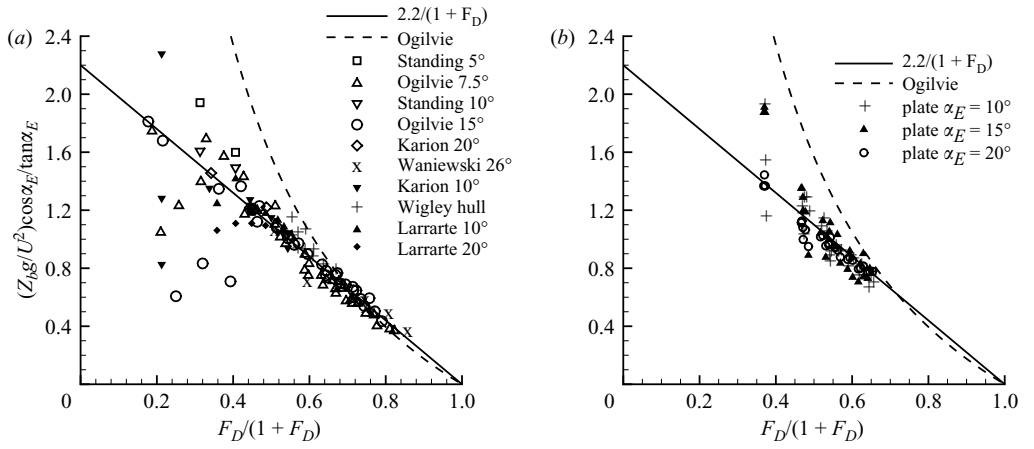

FIGURE 3. Normalized bow wave height $(Z_b g/U^2)\cos\alpha_E/\tan\alpha_E$ for (*a*) ten hull forms, and (*b*) a rectangular flat plate towed at several speeds U, yaw angles α_E and heel angles γ. The straight solid line is the approximation (4.1) and the dashed curve corresponds to Ogilvie's high-Froude-number approximation.

$Z_b \sim 1.6\,\alpha_E\,U\sqrt{D/g}$ obtained by Ogilvie (1973), using a relatively complicated analysis based on matched asymptotic approximations in complementary flow regions, agree except for the factors 2.2 and 1.6. The function $\tan\alpha_E/\cos\alpha_E \sim \alpha_E + 5\alpha_E^3/6$ as $\alpha_E \to 0$ in (4.1) is consistent with thin-ship theory, and was found in Noblesse *et al.* (2006) to yield a slightly better fit to experimental measurements than α_E.

The simple expression (4.1) is compared to experimental measurements in figure 3. This figure depicts the normalized water height $(Z_b g/U^2)\cos\alpha_E/\tan\alpha_E$ as a function of $F_D/(1 + F_D)$, which varies between 0 and 1 for $0 < F_D < \infty$. Figure 3 shows experimental measurements for eight hull forms considered in Noblesse *et al.* (2006), and additional data for two strut-like hulls reported in Larrarte (1994). The simple approximation (4.1), identified by a straight solid line, is in good agreement with most experimental measurements for wedge-shaped ship bows. This approximation is also in fair agreement with measurements for the Wigley hull, for which an effective draught D and an effective waterline entrance angle $2\alpha_E$ were used in accordance with the simple procedure explained in Noblesse *et al.* (2006). A probable reason for the greater scatter of the experimental data at low Froude numbers in figure 3 is that Z_b is small as $U \to 0$ (specifically, $Z_b \propto U^2$) and is divided by U^2. In fact, several of the low-Froude-number experimental data in figure 3(*a*) appear to be outliers; see Noblesse *et al.* (2006). Figure 3(*b*) shows that (4.1) is also consistent with our measurements for a rectangular flat plate. In fact, there are no obvious systematic differences between figures 3(*a*) and 3(*b*). Thus, free-surface flows about a rectangular flat plate at a yaw angle α_E and a hull with wedge-shaped bow and waterline entrance angle $2\alpha_E$ appear to be very similar, at least for small and moderate values of α_E. This experimental result (and the experimental measurements presented further on in figures 8 to 10, 12 and 13) justifies the use – adopted in Noblesse *et al.* (2008) and here – of a flat plate as a (cheap) substitute to a series of ship models for the purpose of generating a relatively large experimental data set. The experimental data in figure 3 are closer to (4.1) than to Ogilvie's high-Froude-number approximation, identified by a dashed curve, except in the range $2 < F_D$ where the two approximations are comparable.

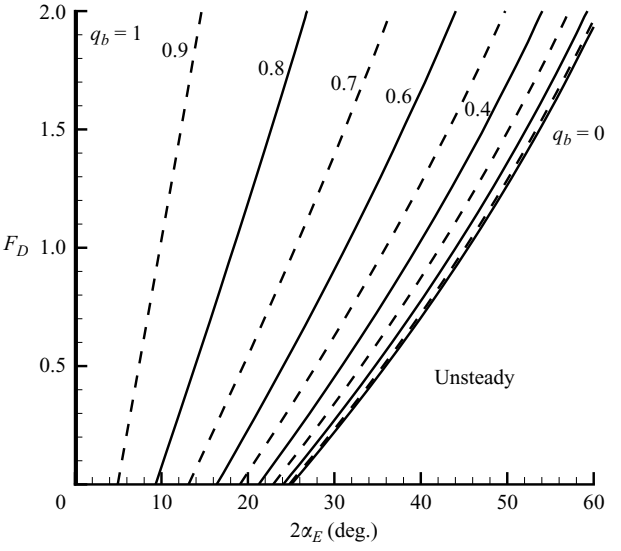

FIGURE 4. Curves $F_D(\alpha_E)$ defined by (5.2) for given values of the total flow velocity q_b at the crest of a ship bow wave.

In summary, the bow wave height Z_b of a ship – having a non-bulbous wedge-shaped bow with a small flare angle – is explicitly defined in terms of the ship speed U, draught D, and waterline entrance angle $2\alpha_E$ by the simple expression (4.1). This expression agrees fairly well with experimental measurements both for hulls with wedge-shaped bows and for a rectangular flat plate.

5. Boundary between unsteady and overturning bow wave regimes

As already noted, two basic types of ship bow wave can be observed: overturning bow waves and unsteady bow waves. The basic issue of predicting whether a ship – that advances at constant speed in calm water – generates an unsteady bow wave or an overturning bow wave is now considered.

The Bernoulli relation (2.3) and equation (4.1) for the height $\zeta = z_b$ of the free surface at the crest of a ship bow wave show that the (total) flow velocity q_b at a bow wave crest is approximately given by

$$q_b^2 = 1 - 2\,z_b \approx 1 - \frac{4.4}{1 + F_D}\,\frac{\tan\alpha_E}{\cos\alpha_E}. \tag{5.1}$$

This equation yields

$$F_D = \frac{4.4}{1 - q_b^2}\,\frac{\tan\alpha_E}{\cos\alpha_E} - 1. \tag{5.2}$$

Equation (5.2) defines a family of curves $F_D(\alpha_E)$ that correspond to specified values of the flow velocity q_b at a bow wave crest. This family of curves is depicted in figure 4 for $q_b = 0, 0.1, \ldots, 0.9, 1$. The curves defined by (5.2) and shown in figure 4 intersect the axis $F_D = 0$ at

$$\alpha_E = \sin^{-1}\left[\sqrt{4.84/\left(1 - q_b^2\right)^2 + 1} - 2.2/\left(1 - q_b^2\right)\right].$$

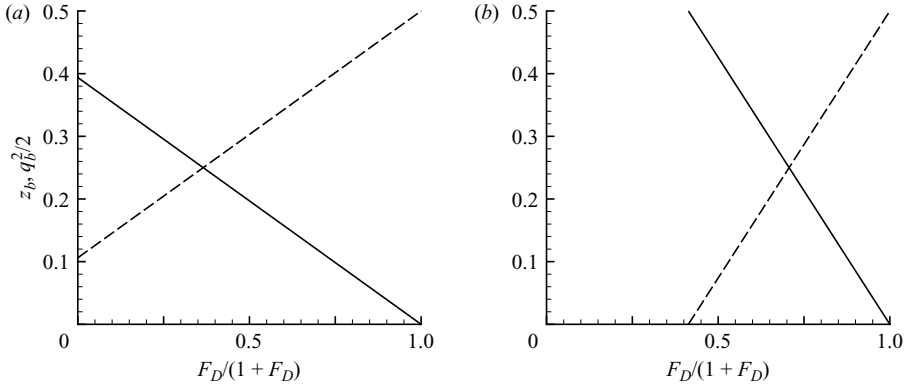

FIGURE 5. Potential energy z_b (———) and kinetic energy $q_b^2/2 = 1/2 - z_b$(– – – –) at the crest of a ship bow wave for (*a*) $\alpha_E = 10^\circ$ and (*b*) $\alpha_E = 20^\circ$. For $\alpha_E = 10^\circ$, an overturning bow wave can exist for every value of F_D. For $\alpha_E = 20^\circ$, no steady overturning bow wave can exist for $F_D/(1+F_D) < 0.4$, i.e. for $F_D < 0.7$.

In particular, we have $2\alpha_E \approx 25^\circ$ for $q_b = 0$, and $\alpha_E \to 0$ as $q_b \to 1$. In the limit $q_b \to 1$, the curve defined by equation (5.2) becomes the vertical axis $\alpha_E = 0$ with $0 < F_D$, as indicated in figure 4.

The region to the right of the curve $q_b = 0$ in figure 4 corresponds to negative values of q_b^2, and to bow wave heights $1/2 < z_b$ that exceed the upper bound $\zeta \leqslant 1/2$ permitted by the Bernoulli relation (2.3) for steady free-surface flows. Thus, no steady bow wave can exist in the region to the right of the curve $q_b = 0$ in figure 4. This curve is defined by (5.2) with $q_b = 0$, i.e.

$$F_D \equiv U/\sqrt{g\,D} = 4.4 \tan\alpha_E / \cos\alpha_E - 1. \tag{5.3}$$

The boundary defined by (5.3) separates two distinct flow regimes: the unsteady bow wave regime and the overturning bow wave regime. In fact, the Bernoulli constraint $\zeta \leqslant 1/2$ for steady free-surface flows precludes steady bow waves in the 'unsteady region' to the right of the curve $q_b = 0$ in figure 4, but does not imply steady flow in the region to the left of the curve $q_b = 0$. Thus, unsteady flow is possible to the left of the curve $q_b = 0$, but steady flow is not possible to the right of the curve $q_b = 0$.

Equation (5.1) yields $z_b \to 0$ and $q_b \to 1$ as $F_D \to \infty$. Thus, the potential energy z_b is null and the kinetic energy $q_b^2/2$ is equal to $1/2$ in this high-Froude-number limit. Equation (5.1) also yields $z_b \to 1/2$ and $q_b^2 \to 0$ along the unsteady flow boundary (5.3). Equation (5.1) shows that the potential energy z_b and the kinetic energy $q_b^2/2$ at the crest of a ship bow wave are linear functions of $F_D/(1+F_D)$. These functions are depicted in figure 5 for $\alpha_E = 10^\circ$ and $\alpha_E = 20^\circ$. For $\alpha_E = 10^\circ$ (figure 5*a*), the kinetic energy $q_b^2/2$ is positive, and an overturning bow wave can exist, for every value of the Froude number F_D. However, for $\alpha_E = 20^\circ$ (figure 5*b*), q_b vanishes for $F_D \approx 0.7$, i.e. for $F_D/(1+F_D) \approx 0.4$, and no steady flow can exist for $F_D < 0.7$.

Figure 6 shows six photographs of waves due to a rectangular flat plate towed at a Froude number $F_D \approx 1.25$ (draught $D = 0.2$ m and speed $U = 1.75\,\mathrm{m\,s^{-1}}$), a heel angle $\gamma = 10^\circ$, and a series of six yaw angles α_E. The values of α_E and F_D that correspond to the photographs in figure 6 are identified by the symbol $\times$ in figure 2. The three photographs on the left-hand side of figure 6 correspond to values of α_E and F_D located on the left-hand side (the overturning bow wave side) of the curve shown in

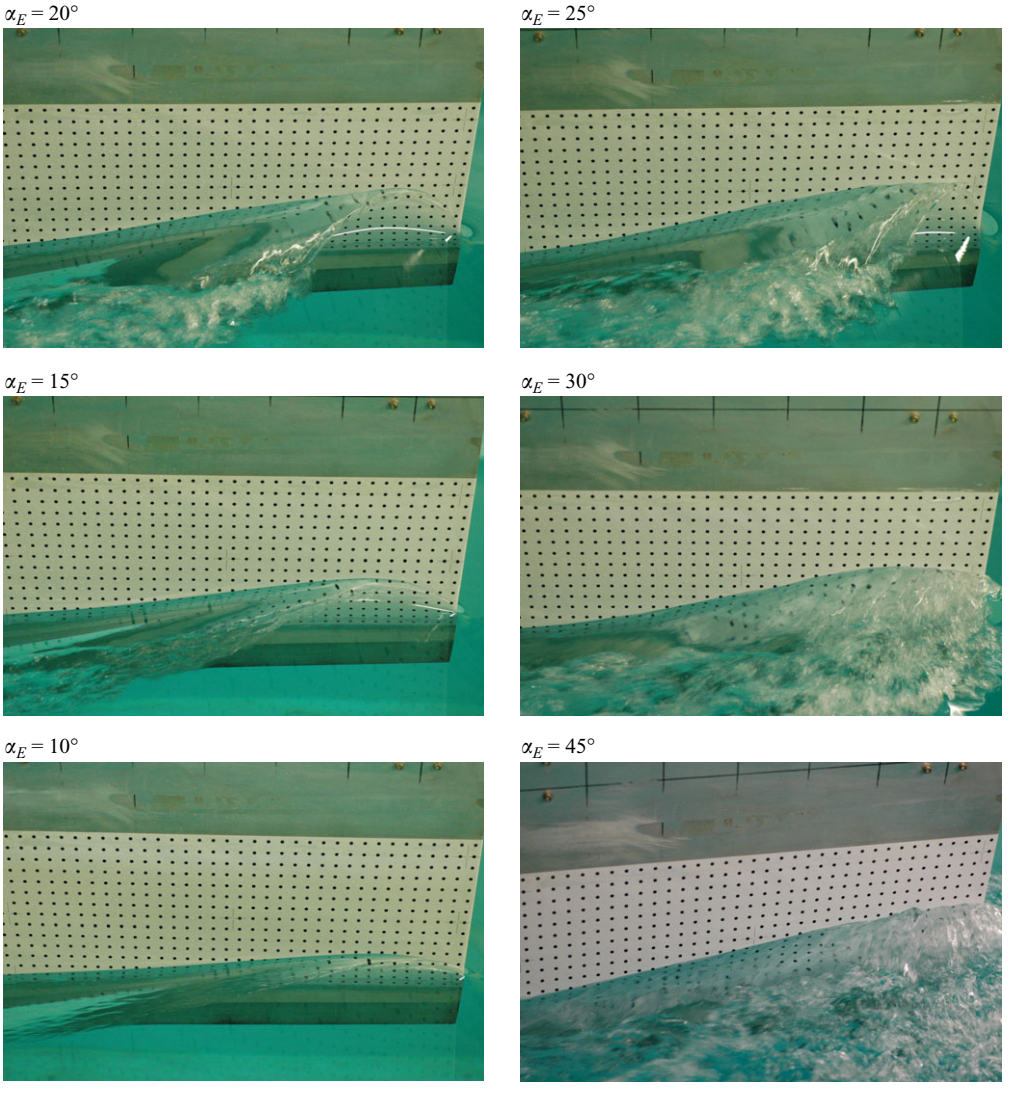

FIGURE 6. Bow waves due to a rectangular flat plate towed at a Froude number $F_D = U/\sqrt{gD} \approx 1.25$ (draught $D = 0.2$ m and speed $U = 1.75\,\mathrm{m\,s^{-1}}$), a heel angle $\gamma = 10°$, and six yaw angles α_E. The values of F_D and α_E that correspond to the six photographs are indicated by $\times$ in figure 2.

figure 2, i.e. the curve $q_b = 0$ in figure 4, and defined by (5.3). The photograph for $\alpha_E = 25°$ in figure 6 corresponds to a point located on the curve in figure 2, and the other two photographs in the right-hand column correspond to points located on the right-hand side (the unsteady bow wave side) of this boundary curve.

The left-hand column of figure 6 shows overturning thin sheets of water (not readily apparent for $\alpha_E = 10°$ because the wave is fairly small). These thin sheets appear to be smooth and steady, until the overturning sheets hit the main body of water and a (turbulent and unsteady) splash is formed. This experimental observation is consistent with the location of the points related to these three photographs on the

left of the boundary curve in figure 2. The overturning wave for $\alpha_E = 10^\circ$ appears to be quite steady, smooth and stable. The photographs of the waves for $\alpha_E = 15^\circ$ and $\alpha_E = 20^\circ$ suggest some degree of instability near the outer edges of the overturning thin sheets of water. The photograph for $\alpha_E = 25^\circ$ is an overturning wave that appears to be less stable than the overturning waves shown in the left-hand column of figure 6. The photograph for $\alpha_E = 30^\circ$, which corresponds to a point located slightly to the right of the boundary curve defined by (5.3) in figure 2, suggests a partly overturning, but highly unsteady, wave. Finally, no overturning is apparent in the highly unsteady and turbulent wave for $\alpha_E = 45^\circ$, which corresponds to a point located well inside the 'unsteady region' on the right of the boundary curve in figure 2.

Thus, figure 6 documents a gradual transition from a highly stable overturning thin sheet of water for $\alpha_E = 10^\circ$ to a highly unsteady and turbulent wave for $\alpha_E = 45^\circ$, and a gradual decrease in flow unsteadiness as the boundary curve in figure 2 is crossed from right to left. Furthermore, the three photographs in the left-hand column of figure 6 suggest that flow unsteadiness gradually moves upward along the overturning thin sheet of water, until it reaches the plate in the top right corner of figure 6. Thus, the boundary curve defined by (5.3) appears to correspond to the limiting case when flow unsteadiness occurs at the plate (or ship hull), rather than at some distance away from the plate for points located on the left side of the curve in figure 2.

In summary, a ship with a sufficiently fine waterline, specifically with waterline entrance angle $2\alpha_E$ smaller than approximately 25°, may generate an overturning bow wave at any speed. However, a ship with a fuller waterline, for $25^\circ < 2\alpha_E$, can only generate an overturning bow wave if the ship speed is higher than the critical speed defined by (5.3). This simple expression explicitly defines the boundary between the unsteady and overturning bow wave regimes in terms of the ship speed U, draught D, and waterline entrance angle $2\alpha_E$. The boundary curve that separates the unsteady and overturning bow wave regimes corresponds to the special case for which the flow velocity q_b at the crest of a ship bow wave is null. This property provides a simple physical interpretation of the transition between overturning and unsteady bow waves. A water particle at the crest of a wave (or a ball at the top of a mound) without momentum is not stable. In this case, a ship bow wave can be expected to be highly unsteady, and to move back and forth in the vicinity of the ship bow. The curves that correspond to increasingly higher values of the flow velocity q_b at a bow wave crest can be presumed to correspond to increasingly more stable and steady overturning bow waves. Thus, figure 4 defines regions where ship bow waves can be expected to be unsteady, or increasingly more steady and stable.

The definition of the 'steady overturning bow wave regime' and the 'unsteady bow wave regime' that is used here is based on a simple theoretical argument (flow velocity at the bow wave crest given by the Bernoulli relation). This definition is a 'theoretical' definition, rather than an 'experimental' definition based on observed flow characteristics. Nevertheless, our flow observations, notably those reported in figure 6, for a rectangular flat plate towed at several speeds and yaw angles are consistent with figure 4. Overturning bow waves in the (α_E, F_D) region that is very close to the unsteady boundary curve $q_b = 0$ in figure 4, i.e. for small wave crest velocity q_b, exhibit considerable unsteadiness. On the contrary, overturning bow waves observed in the (α_E, F_D) region well to the left of the curve $q_b = 0$ are stable and steady thin sheets of water (until the plunging wave hits the main body of water).

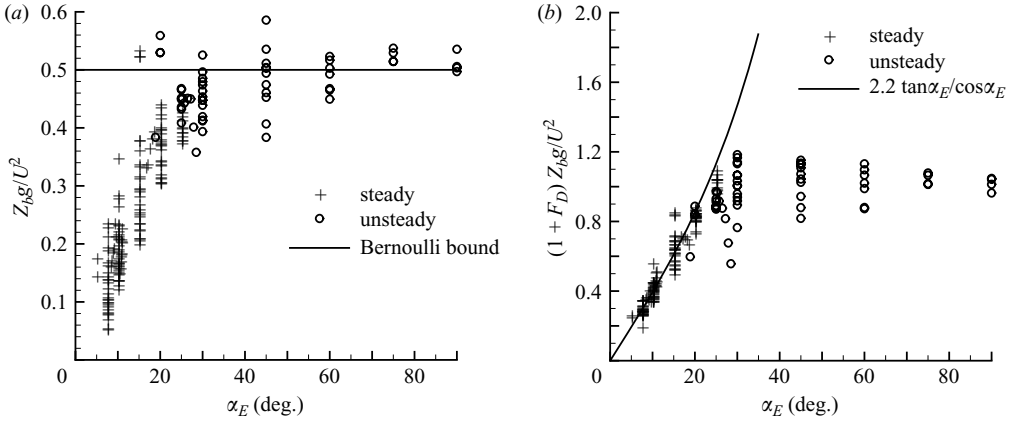

FIGURE 7. Normalized bow wave heights $Z_b g/U^2$ (*a*) and (*b*) $(1+F_D)Z_b\, g/U^2$ as functions of the waterline half entrance angle, or yaw angle, α_E. The experimental measurements shown in figure 7 include data for eleven hull forms and flat-plate data. The data identified by $\circ$ or $+$ correspond to values of α_E and F_D in the unsteady or steady flow regions on the right or left sides, respectively, of the boundary curve $q_b = 0$ in figure 4.

6. Height of an unsteady ship bow wave

A ship with a large waterline entrance angle α_E (specifically, for $25^\circ < 2\alpha_E$) was shown in the previous section to generate an unsteady bow wave, except when F_D is sufficiently large. The height Z_b of an unsteady ship bow wave is now considered.

Figures 7(*a*) and 7(*b*) show the bow wave heights $Z_b\, g/U^2$ and $(1+F_D)Z_b g/U^2$, respectively, as functions of the waterline half entrance angle, or yaw angle, α_E. The experimental measurements shown in figure 7 include all the data (flat-plate data for yaw angles $\alpha_E = 10^\circ$, 15°, 20°, and data for ten hull forms) considered in figure 3. In addition, figure 7 shows data for the Larrarte 30° strut-like hull, and flat-plate data for yaw angles $\alpha_E = 25^\circ$, 30°, 45°, 60°, 75°, 90°. A relatively large number of experimental measurements is then considered. The data are divided into two groups, identified by $\circ$ or $+$, which correspond to values of α_E and F_D in the unsteady or 'steady' (overturning wave) flow regions on the right or left sides, respectively, of the (zero wave crest velocity) boundary curve $q_b = 0$ defined by (5.3) and shown in figure 4. Thus, this division into 'steady' and 'unsteady' data is not based on flow observations, but strictly upon the location of α_E and F_D to the left or right sides of the boundary curve $q_b = 0$ shown in figure 4.

Figure 7(*a*) shows that the 'steady-flow' data lie below the horizontal line $Z_b\, g/U^2 = 1/2$, in agreement with the Bernoulli constraint $Z_b\, g/U^2 \leqslant 1/2$ for steady free-surface flows. Figure 7(*a*) also shows that the 'unsteady-flow' data are distributed, more or less evenly, above and below the horizontal line $Z_b\, g/U^2 = 1/2$. Thus, the height Z_b of an unsteady ship bow wave is approximately equal to the upper bound

$$z_b \equiv Z_b g/U^2 = 1/2, \tag{6.1}$$

allowed by the Bernoulli relation for steady free-surface flows. Figure 7(*b*) shows that the 'steady-flow' data are distributed, fairly evenly, around the curve $2.2\tan\alpha_E/\cos\alpha_E$, in accordance with the approximation (4.1) and figure 3. Figure 7(*b*) also shows that the 'unsteady-flow' data are located below the curve $2.2\tan\alpha_E/\cos\alpha_E$. Thus, (4.1) and (6.1) provide reasonable approximations for the height Z_b of a ship bow wave in the overturning and unsteady flow regimes. Furthermore, figure 7 shows that

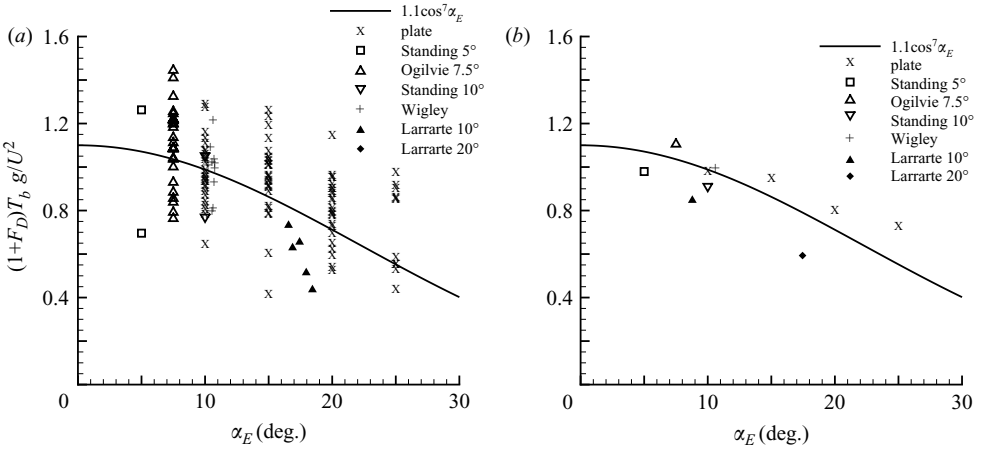

FIGURE 8. Normalized distance $(1 + F_D)\, T_b g/U^2$ between a ship stem and bow wave crest for six hull forms and a flat plate. The curve is the approximation $1.1\cos^7\alpha_E$ related to (7.1). The points in (*b*) are the centroids of the scattered experimental measurements shown in (*a*).

these expressions also provide upper bounds for Z_b in the unsteady and overturning regimes, respectively.

In summary, (4.1) and (6.1) and figure 7 show that the height Z_b of the bow wave of a ship with a non-bulbous wedge-shaped bow is approximately given by

$$z_b \equiv \frac{Z_b g}{U^2} \approx \min\left(\frac{2.2}{1+F_D}\,\frac{\tan\alpha_E}{\cos\alpha_E}, \frac{1}{2}\right). \tag{6.2}$$

Figure 7 shows that this simple expression is in reasonable agreement with experimental measurements both for hulls with wedge-shaped bows and for a flat plate. Equation (6.2) directly defines the height Z_b of a ship bow wave, which may be overturning or unsteady, in terms of the ship speed U, draught D, and waterline entrance angle $2\alpha_E$.

7. Distance between a ship stem and bow wave crest

The distance T_b (measured along the ship hull surface) between a ship stem and bow wave crest is now considered. The fundamental theoretical considerations (dimensional analysis and rudimentary asymptotic considerations in the shallow-draught and deep-draught limits) used in Noblesse *et al.* (2006) show that the function $t_b^* \equiv (1 + F_D)T_b\, g/U^2$ can be expected to be independent of the ship draught D and speed U. Thus, t_b^* is presumed to depend only on the waterline entrance angle α_E. Furthermore, experimental observations and symmetry considerations suggest that the function $t_b^*(\alpha_E)$ may be assumed to vanish in the limit $\alpha_E \to 90°$.

Figure 8(*a*) shows the normalized distance t_b^* between a ship stem and bow wave crest as a function of α_E for six hull forms and a rectangular flat plate. Only experimental measurements in the 'steady' flow (overturning wave) side of the boundary curve defined by (5.3) and identified as the (zero wave crest velocity) curve $q_b = 0$ in figure 4, are considered in figure 8. The points in figure 8(*b*) are the centroids of the scattered experimental measurements shown in figure 8(*a*). Figure 8 shows that the curve $1.1\cos^7\alpha_E$ provides a reasonable fit to the experimental measurements. This

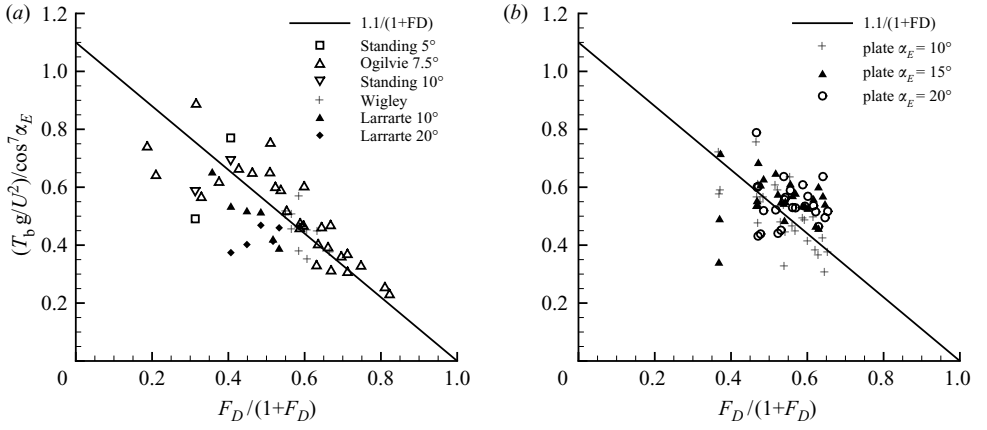

FIGURE 9. Normalized distance $(T_b g/U^2)/\cos^7\alpha_E$ between a ship stem and bow wave crest for six hull forms (*a*) and (*b*) a flat plate. The straight line is the approximation $1.1/(1+F_D)$ related to (7.1).

curve corresponds to the approximation

$$t_b \equiv T_b\, g/U^2 \approx 1.1(\cos^7\alpha_E)/(1+F_D). \tag{7.1}$$

This simple approximation is also depicted in figure 9, where the normalized distance $(T_b g/U^2)/\cos^7\alpha_E$ is shown as a function of $F_D/(1+F_D)$. Figures 9(*a*) and 9(*b*) show experimental measurements for six hull forms and a flat plate, respectively. In the high-Froude-number-thin-ship limit $F_D \to \infty$ and $\alpha_E \to 0$, (7.1) yields $T_b \sim 1.1\, U\sqrt{D/g}$.

In summary, the distance T_b between the stem and the bow wave crest of a ship with a non-bulbous wedge-shaped bow is explicitly defined in terms of the ship speed U, draught D, and waterline entrance angle $2\alpha_E$ by (7.1). This expression is in reasonable agreement with experimental data both for hulls with wedge-shaped bows and for a flat plate. For small waterline entrance angle α_E, (7.1) agrees with the expression $T_b\, g/U^2 \approx 1.1/(1+F_D)$ given in Noblesse *et al.* (2006).

8. Rise of water at a ship stem

The simple expression for the rise Z_s of water at a ship stem given in Noblesse *et al.* (2008) is required further on, and thus is now briefly considered. The water height Z_s is measured from the horizontal plane $Z=0$ of the undisturbed free surface, as shown in figure 1. The water height Z_s at a ship stem is considered in Noblesse *et al.* (2008) using two methods: thin-ship theory (a fully analytical approach) and a theoretical–experimental approach based on both fundamental theoretical considerations (dimensional analysis, and rudimentary asymptotic considerations in the shallow-draught and deep-draught limits) and experimental measurements, in a manner similar to that used for the bow wave height Z_b in Noblesse *et al.* (2006). Both the theoretical–experimental method and thin-ship theory yield simple relations. Furthermore, these relations are in close agreement, except for $F_D \ll 1$.

Specifically, the thin-ship analysis considered in Noblesse *et al.* (2008) yields

$$z_s \equiv \frac{Z_s\, g}{U^2} \approx \frac{2}{\pi}\,\frac{\tan\alpha_E}{\cos\alpha_E}\,E^s(F_D) \tag{8.1}$$

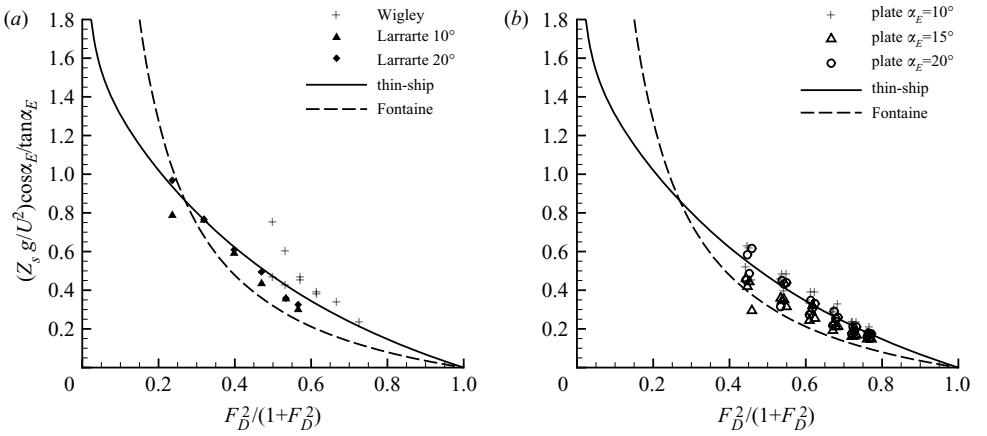

FIGURE 10. Normalized water height $(Z_s\, g/U^2)\cos\alpha_E\,/\tan\alpha_E$ at a ship stem for (*a*) three hull forms, and (*b*) a rectangular flat plate towed at several speeds U, yaw angles α_E and heel angles γ. The solid line and the dashed curve correspond to the thin-ship approximation (8.1) and Fontaine's high-Froude-number approximation, respectively.

with

$$E^s(F_D) \equiv \int_0^{\pi/2} \mathrm{d}t\, \left[1-\exp\left(-(\sin^2 t)/F_D^2\right)\right]/\sin t.$$

This integral can be approximated as

$$E^s \approx \frac{1}{1+F_D^2} + \frac{2/3}{\left(1+F_D^2\right)^2} + \frac{19/45}{\left(1+F_D^2\right)^3} + \frac{26/105}{\left(1+F_D^2\right)^4} + \frac{601/4725}{\left(1+F_D^2\right)^5} + \frac{1502/31185}{\left(1+F_D^2\right)^6} + 4.16\exp(-13F_D - 0.26). \tag{8.2}$$

The series in (8.2) is a (modified) high-Froude-number asymptotic expansion. This series is nearly identical to the integral E^s for $0.3 \leqslant F_D$. The last term in expression (8.2) is a low-Froude-number correction. Equation (8.2) closely approximates the function E^s, except for $F_D \ll 1$, and can then be used in practice (Noblesse *et al.* 2008).

In the high-Froude-number-thin-ship limit $F_D \to \infty$ and $\alpha_E \to 0$, (8.1) and (8.2) yield $Z_s \sim 2\,\alpha_E D/\pi$. This approximation and the high-Froude-number approximation $Z_s \sim \alpha_E D/\pi$ obtained by Fontaine *et al.* (2000), using matched complementary asymptotic approximations in a manner similar to that used by Ogilvie (1973), are in agreement except for a factor 2. The function $\tan\alpha_E/\cos\alpha_E$ in (8.1) is consistent with thin-ship theory, and is shown in Noblesse *et al.* (2008) to fit experimental measurements slightly better than α_E.

The simple expression (8.1) is compared to experimental measurements in figure 10. This figure depicts the normalized water height $(Z_s g/U^2)\cos\alpha_E\,/\tan\alpha_E$ as a function of $F_D^2/(1+F_D^2)$, which varies between 0 and 1 for $0 < F_D < \infty$. Figure 10(*a*) shows experimental measurements, reported in Kajitani *et al.* (1983) and Larrarte (1994), for the Wigley hull and two strut-like hulls. Figure 10(*b*) shows measurements for a rectangular flat plate. There are no obvious systematic differences between figures 10(*a*) and 10(*b*). This experimental result, already observed in figures 3, 8 and 9, further supports the use – adopted in Noblesse *et al.* (2008) and here – of a flat plate (as a cheap substitute to a series of ship models) to generate a relatively large set of experimental measurements. Equation (8.1), identified by a solid line,

is in good agreement with the measurements considered in figure 10. In fact, these measurements are fairly evenly distributed around the thin-ship approximation (8.1). Fontaine's high-Froude-number approximation, shown as a dashed curve, lies below most measurements.

In summary, the rise Z_s of water at the stem of a ship with a non-bulbous wedge-shaped bow is explicitly defined in terms of the ship speed U, draught D, and waterline entrance angle $2\alpha_E$ by the simple expressions (8.1) and (8.2). These expressions agree fairly well with experimental measurements both for hulls with wedge-shaped bows and for a rectangular flat plate.

9. Bow wavefront

The height Z_b of a ship bow wave, the distance T_b between a ship stem and the bow wave crest, and the water rise Z_s at the ship stem have already been considered in §§ 4 and 6–8. The front of a ship bow wave, i.e. the portion of the wave located between the ship stem and the wave crest, is now considered further.

The magnitude q_s of the flow velocity at a ship stem is defined, via the Bernoulli relation (2.3), in terms of the elevation z_s of the free surface at the stem as

$$q_s = \sqrt{1 - 2\,z_s}. \tag{9.1}$$

Let $t = T\,g/U^2$ stand for the non-dimensional distance, measured from the ship stem, along a horizontal axis that is tangent to the mean ship waterline at the ship stem, and points toward the ship stern. Thus, the free surface intersects the ship stem at $t = 0$ and $z = z_s$. Furthermore, define the non-dimensional time $\theta = \Theta\,g/U$, and let β stand for the angle between the horizontal mean free-surface plane and the (total) flow velocity at the ship stem. The components, along the horizontal t-axis and the vertical z-axis, of the flow velocity at the stem are then given by $q_s \cos\beta$ and $q_s \sin\beta$, respectively.

A simple approximation for the front of a ship bow wave profile can be obtained by assuming that a water particle that passes the stem ($t = 0, z = z_s$) follows a path determined by Newton's equations $\mathrm{d}^2t/\mathrm{d}\theta^2 = 0$ and $\mathrm{d}^2z/\mathrm{d}\theta^2 = -1$. This elementary Lagrangian analysis, which ignores interactions among water particles, shows that the path of a water particle is defined by

$$t = \theta\,q_s \cos\beta,\ z = z_s + \theta\,q_s \sin\beta - \theta^2/2.$$

Here, a water particle is assumed to be located at the ship stem ($t = 0, z = z_s$) at time $\theta = 0$. The foregoing parametric equations yield

$$z = z_s + \frac{t}{q_s^2 \cos^2\beta}\left(q_s^2 \sin\beta \cos\beta - \frac{t}{2}\right). \tag{9.2}$$

Thus, we have $z = z_s$ for $t = 0$ and for $t = 2\,q_s^2 \sin\beta \cos\beta$. Equation (9.2) shows that the highest value of z is reached at $t = t_b = q_s^2 \sin\beta \cos\beta$ and is given by $z_b = z_s + (q_s \sin\beta)^2/2$. It follows that we have $q_s \sin\beta = \sqrt{2(z_b - z_s)}$. This relation and (9.1) yield $q_s \cos\beta = \sqrt{1 - 2\,z_b}$ and

$$t_b \equiv T_b\,g/U^2 = \tau_b \sqrt{1 - h_b^s}. \tag{9.3}$$

In this expression, which provides an alternative to (7.1), τ_b is defined as

$$\tau_b = \sqrt{2\,z_b(1 - 2\,z_b)}, \tag{9.4}$$

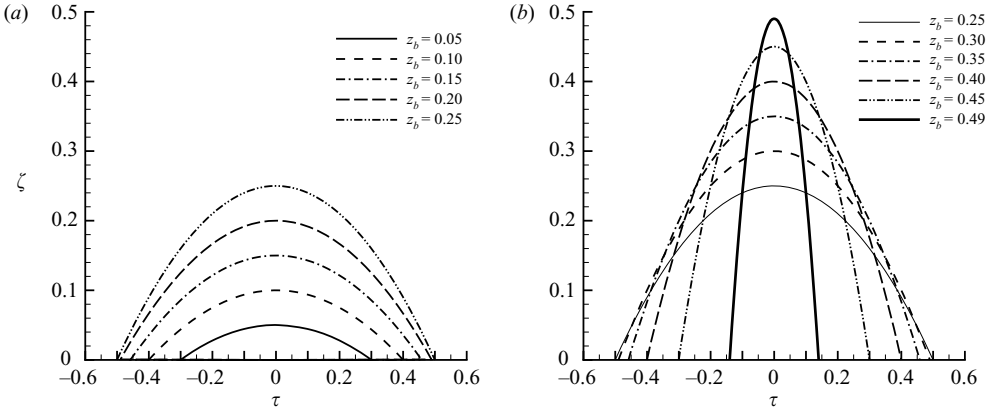

FIGURE 11. Family of parabolic bow waves defined by (9.4) and (9.7) for (*a*) $z_b = 0.05$, 0.1, 0.15, 0.2, 0.25 and (*b*) $z_b = 0.25$, 0.3, 0.35, 0.4, 0.45, 0.49.

and $h_b^s \equiv z_s/z_b$ is defined by (6.2) and (8.1) as

$$h_b^s \equiv \frac{Z_s}{Z_b} \approx \min\left(\frac{1+F_D}{3.5}\, E^s(F_D),\, 1\right), \tag{9.5}$$

where the function $E^s(F_D)$ is given by (8.2). The upper bound 1 in (9.5), required in (9.3), is shown in Noblesse *et al.* (2008) to be consistent with experimental observations and (6.2) and (8.1), except at very low Froude numbers F_D. Equation (9.3) yields $t_b \leqslant \tau_b$, $t_b = \tau_b$ if $z_s = 0$, and $t_b \approx \tau_b$ if $h_b^s \ll 1$. Equation (9.2), the relations $q_s^2 \sin\beta\cos\beta = t_b$ and $q_s^2\cos^2\beta = 1 - 2\,z_b$, and (9.3) and (9.4), yield

$$\zeta/z_b = h_b^s + (1-h_b^s)(2 - t/t_b)t/t_b \quad \text{for } 0 \leqslant t \leqslant t_b. \tag{9.6}$$

Here, ζ is used instead of z to emphasize that (9.6) defines the location $z = \zeta$ of the free surface.

The change of variable $t = \tau + t_b$, which places the origin $\tau = 0$ at the bow wave crest, in (9.6) yields

$$\zeta/z_b = 1 - \tau^2/\tau_b^2. \tag{9.7}$$

Equations (9.7) and (9.4) define a family of parabolic ship bow waves that is entirely defined in terms of the height z_b of the bow wave. This simple one-parameter analytical family of bow waves is depicted for $z_b = 0.05$, 0.1, 0.15, 0.2, 0.25 (figure 11*a*) and for $z_b = 0.25$, 0.3, 0.35, 0.4, 0.45, 0.49 (figure 11*b*). In the limit $z_b = 0.5$, (9.4) predicts that the width of the bow wave vanishes, and the wave (9.7) becomes a vertical wall of water. Thus, the bow wave (9.7) becomes a (clearly unstable) vertical wall as the wave height z_b approaches the upper bound $z_b = 0.5$ allowed by the Bernoulli relation for steady flows. This property provides further insight into the unsteady-flow boundary (5.3), already shown to correspond to the special case when the flow velocity q_b at the bow wave crest is null.

In summary, (9.6), (6.2), (9.5), (9.4) and (9.3) define the front $0 \leqslant t \leqslant t_b$ of the bow wave of a ship with a non-bulbous wedge-shaped bow directly in terms of the ship speed U, draught D, and waterline entrance angle $2\alpha_E$. For an unsteady bow wave, we have $z_b = 1/2$ and the wavefront defined by (9.6) is a vertical wall $t_b = 0$ with $z_s \leqslant \zeta \leqslant 1/2$. These simple expressions for the front of a ship bow wave are compared to experimental measurements in § 11, where the profile of a ship bow wave beyond the bow wave crest, i.e. for $t_b < t$, is also considered.

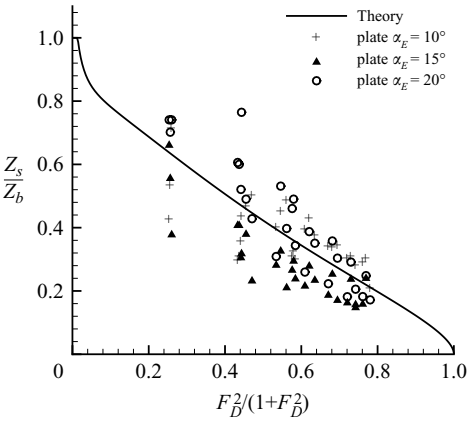

FIGURE 12. Ratio Z_s/Z_b of the rise Z_s of water at a ship stem to the bow wave height Z_b for a flat plate towed at several speeds U, yaw angles α_E and heel angles γ. The solid line corresponds to the analytical expression (9.5).

10. Comparison of theoretical expressions to measurements

Expressions (9.5) and (8.2) for the ratio Z_s/Z_b of the rise of water Z_s at a ship stem to the bow wave height Z_b, and the two alternative expressions (7.1) or (9.3)–(9.5) with (6.2) for the distance T_b between the stem and the bow wave crest of a ship, are now compared to experimental measurements.

Equation (9.5), with (8.2), is compared to experimental measurements for a rectangular flat plate in figure 12, where the ratio Z_s/Z_b is depicted as a function of $F_D^2/(1+F_D^2)$. The experimental measurements are distributed fairly evenly above and below the theoretical curve defined by the simple expression (9.5). The scatter of the experimental measurements in figure 12 is probably due to the compounding of experimental uncertainties associated with two measurements (Z_s and Z_b) and to the fact that Z_b and (especially) Z_s are relatively small for the yaw angles $10° \leqslant \alpha_E \leqslant 20°$ considered in figure 12.

Figure 13 depicts $\tau_b \equiv (T_b\, g/U^2)/\sqrt{1 - Z_s/Z_b}$ as a function of $z_b \equiv Z_b\, g/U^2$. The circle in this figure corresponds to (9.4). This simple expression is compared to experimental measurements for three hulls with wedge-shaped bows (figure 13*a*) and a rectangular flat plate (figure 13*b*). The scatter of the experimental measurements in figure 13 is probably due to the compounding of experimental uncertainties associated with three measurements (T_b, Z_b and Z_s) and the fact that experimental uncertainties are larger for T_b than for Z_b. The circle in figure 13 fits the experimental measurements reasonably well for $\alpha_E = 20°$ and $\alpha_E = 15°$, but not so well for $\alpha_E = 10°$.

The two alternative expressions for the distance T_b between the stem and the bow wave crest of a ship given by (7.1) and by (9.3)–(9.5) with (6.2) and (8.2) are compared in figure 14. Specifically, figures 14(*a*) and 14(*b*) depict $(T_b\, g/U^2)/\sqrt{1 - Z_s/Z_b}$ as a function of $Z_b\, g/U^2$, or $(T_b\, g/U^2)/\cos^7 \alpha_E$ as a function of $F_D/(1 + F_D)$, respectively. In figure 14(*a*), the circle corresponds to (9.4), and the three curves identified as $\alpha_E = 10°$, 15°, 20° correspond to (7.1). In figure 14(*b*), the straight line corresponds to (7.1), and the three curves identified as $\alpha_E = 10°$, 15°, 20° correspond to (9.3)–(9.5), (6.2), (8.2). Experimental measurements for a rectangular flat plate at yaw angles $\alpha_E = 10°$, 15°, 20° are also shown in figure 14. The measurements for $\alpha_E = 10°$ are in better agreement with (7.1) than with (9.3)–(9.5), (6.2), (8.2). The reverse appears

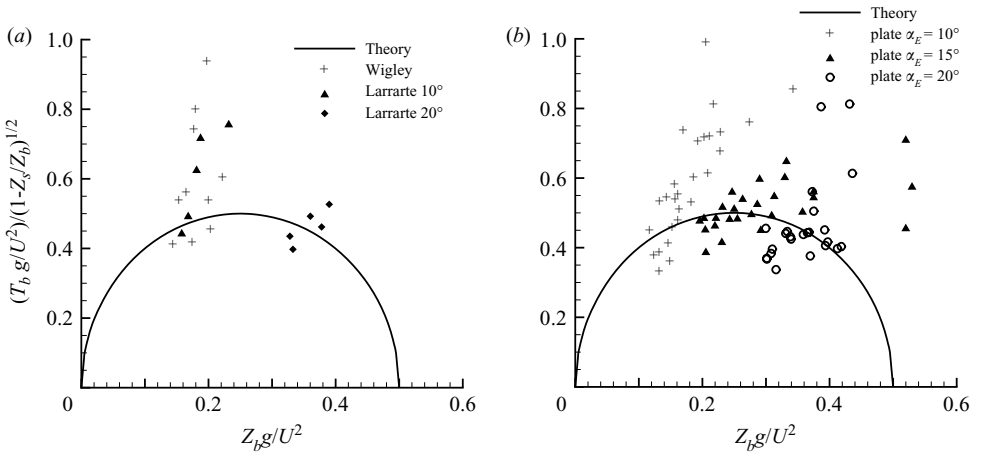

FIGURE 13. Comparison of the circle defined by (9.3) and (9.4) to experimental measurements for (*a*) three hulls with wedge-shaped bows and (*b*) a rectangular flat plate.

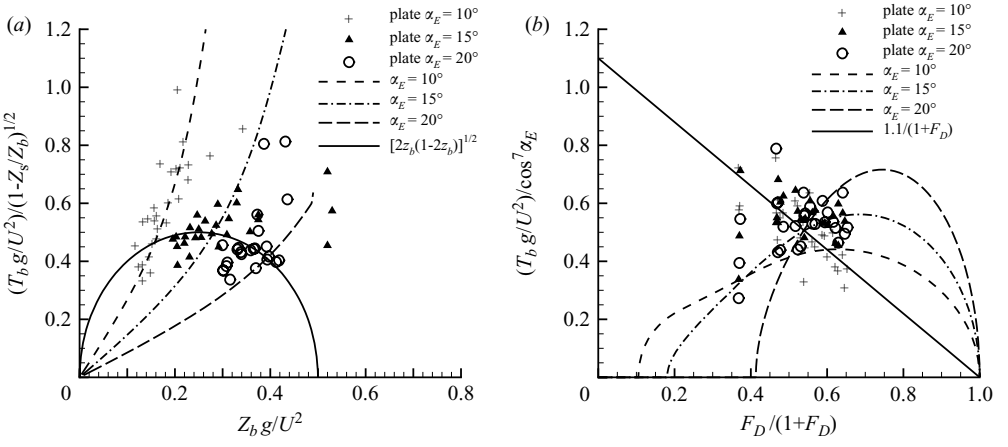

FIGURE 14. Comparison of the two alternative expressions for the distance T_b between a ship stem and bow wave crest given by (7.1) and (9.3), (9.4), (9.5), (6.2), (8.2) to experimental measurements for a rectangular flat plate. The circle (*a*) and the straight line (*b*) correspond to expressions (9.4) and (7.1), respectively. The three curves identified as $\alpha_E = 10°$, 15° and 20° correspond to (7.1) or (9.3)–(9.5), (6.2), (8.2) in (*a*) and (*b*), respectively.

to hold for $\alpha_E = 20°$ and $\alpha_E = 15°$, although this conclusion can only be tentative in view of the scatter of the experimental data.

In summary, figures 12 to 14 show that expressions (9.5) and (8.2) for the ratio Z_s/Z_b of the rise Z_s of water at a ship stem to the bow wave height Z_b, and the alternative expressions for the distance T_b between a ship stem and bow wave crest given by (7.1) or (9.3)–(9.5) and (6.2) are in reasonable agreement with experimental measurements.

11. Ship bow wave profile

The front of the bow wave is entirely determined – via a highly-simplified Lagrangian analysis (given in § 9) that ignores interactions among water particles

– in terms of the water rise z_s at the ship stem and the related flow velocity q_s given by the Bernoulli relation (9.1). The thin-ship analysis of the water rise z_s at a ship stem given in Noblesse *et al.* (2008) shows that the water elevation z_s stems from integration – over the ship hull surface – of the local-flow component in the expression for the Green function that satisfies the Michell linearized free-surface boundary condition. Thus, the water rise z_s at a ship stem and the bow wavefront correspond to a 'near-field flow effect', which is closely related to the ship-hull boundary condition, and in fact accounts for the obstruction of the ship hull in the uniform current $(-U, 0, 0)$ that opposes the ship speed.

This 'physical interpretation' of the elementary analysis of the front of a ship bow wave shows that the parabolic bow wavefront is strongly influenced by the boundary condition at the ship hull, and thus corresponds to a 'nearfield wave'. In fact, the front of a ship bow wave is similar to the front of a wave generated by a wavemaker. However, the flow beyond the crest of a wave – generated by a ship bow or a wavemaker in a tank – is not as strongly affected by the near-field boundary condition at the ship hull or at the wavemaker, and indeed essentially corresponds to a 'free wave', i.e. a plane progressive wave. Specifically, a ship bow wave aft of the wave crest can be expected to be reasonably approximated by an elementary plane wave alongside the hull, with wavelength $2\pi(\cos^2\alpha_E)U^2/g$, i.e. $\zeta/z_b = \cos[(t-t_b)/\cos^2\alpha_E]$.

This sinusoidal approximation and the parabolic approximation (9.6) yield

$$\left.\begin{aligned} \zeta/z_b &= h_b^s + \big(1-h_b^s\big)(2-t/t_b)t/t_b \quad \text{for} \quad 0 \leqslant t \leqslant t_b, \\ \zeta/z_b &= \cos[(t-t_b)/\cos^2\alpha_E] \qquad\quad \text{for} \quad t_b \leqslant t, \end{aligned}\right\} \tag{11.1a}$$

where the alternative expressions

$$\left.\begin{aligned} t_b &= \sqrt{2\,z_b(1-2\,z_b)\big(1-h_b^s\big)} \equiv t_b(z_b), \\ t_b &= 1.1\,(\cos^7\alpha_E)/(1+F_D) \equiv t_b(F_D), \end{aligned}\right\} \tag{11.1b}$$

for the distance t_b between the ship stem and the bow wave crest may be used, and the bow wave height z_b and the ratio $h_b^s = z_s/z_b$ of the water rise z_s at the ship stem over the bow wave height are defined by (6.2) and (9.5) as

$$z_b \equiv \frac{Z_b g}{U^2} \approx \min\left(\frac{2.2}{1+F_D}\,\frac{\tan\alpha_E}{\cos\alpha_E}, \frac{1}{2}\right), \tag{11.1c}$$

$$h_b^s \equiv \frac{Z_s}{Z_b} \approx \min\left(\frac{1+F_D}{3.5}\,E^s(F_D), 1\right), \tag{11.1d}$$

with the function $E^s(F_D)$ given by (8.2). The simple analytical expressions (11.1) directly define a ship bow wave profile in terms of the ship speed U, draught D, and waterline entrance angle $2\alpha_E$. The notation $t_b(z_b)$ and $t_b(F_D)$ in (11.1*c*) is used as a convenient way of identifying the two sets of curves in figures 15–21.

In summary, (11.1) represents a ship bow wave in terms of two complementary pieces: a (nonlinear) parabolic wavefront (between a ship stem and bow wave crest), influenced by near-field effects (specifically, the boundary condition at the ship hull), and a (linear) sinusoidal elementary 'free' wave. Equations (11.1) and (8.2) provide a simple analytical approximation that directly defines the bow wave profile of a ship with a non-bulbous wedge-shaped bow in terms of the ship speed U, draught D, and waterline-entrance angle $2\alpha_E$.

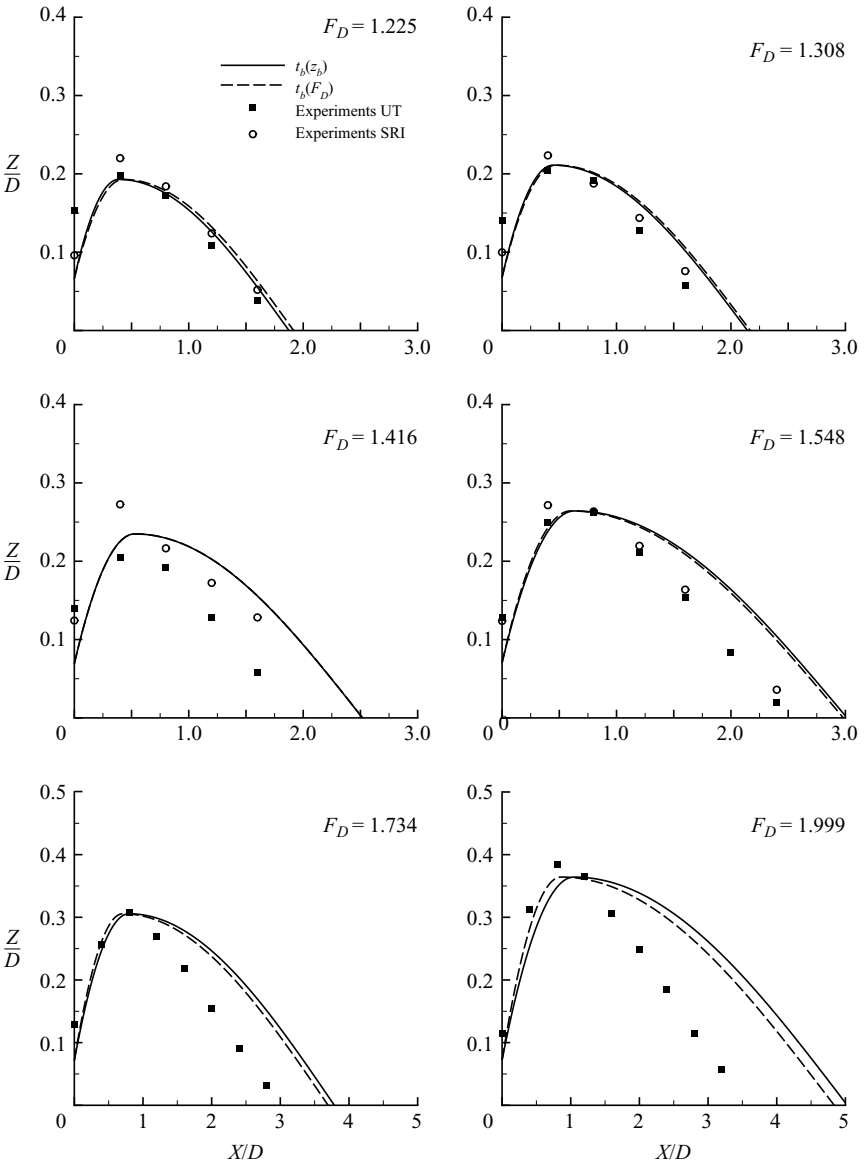

FIGURE 15. Theoretical bow wave profiles (11.1) and experimental measurements reported in Kajitani *et al.* (1983) for the Wigley hull. The draught-based Froude numbers F_D considered in this figure correspond to length-based Froude numbers equal to 0.250, 0.267, 0.289, 0.316, 0.354 and 0.408.

12. Comparison of analytical and experimental bow wave profiles

These expressions are compared to experimental measurements in figures 15–21 for the Wigley hull, the series of three strut-like hulls with sharp-ended parabolic waterlines and entrance angles $2\alpha_E = 20°$, $40°$, $60°$ considered by Larrarte (1994), and a rectangular flat plate towed at yaw angles $\alpha_E = 10°$, $20°$, $30°$. Figure 15 for the Wigley hull shows two sets of experimental measurements, obtained at the University of Tokyo (UT) and the Ship Research Institute (SRI) in Japan. Figures 17, 19 and 21 show our measurements for a flat plate towed at heel angles $\gamma = 0°$, $10°$ and $15°$,

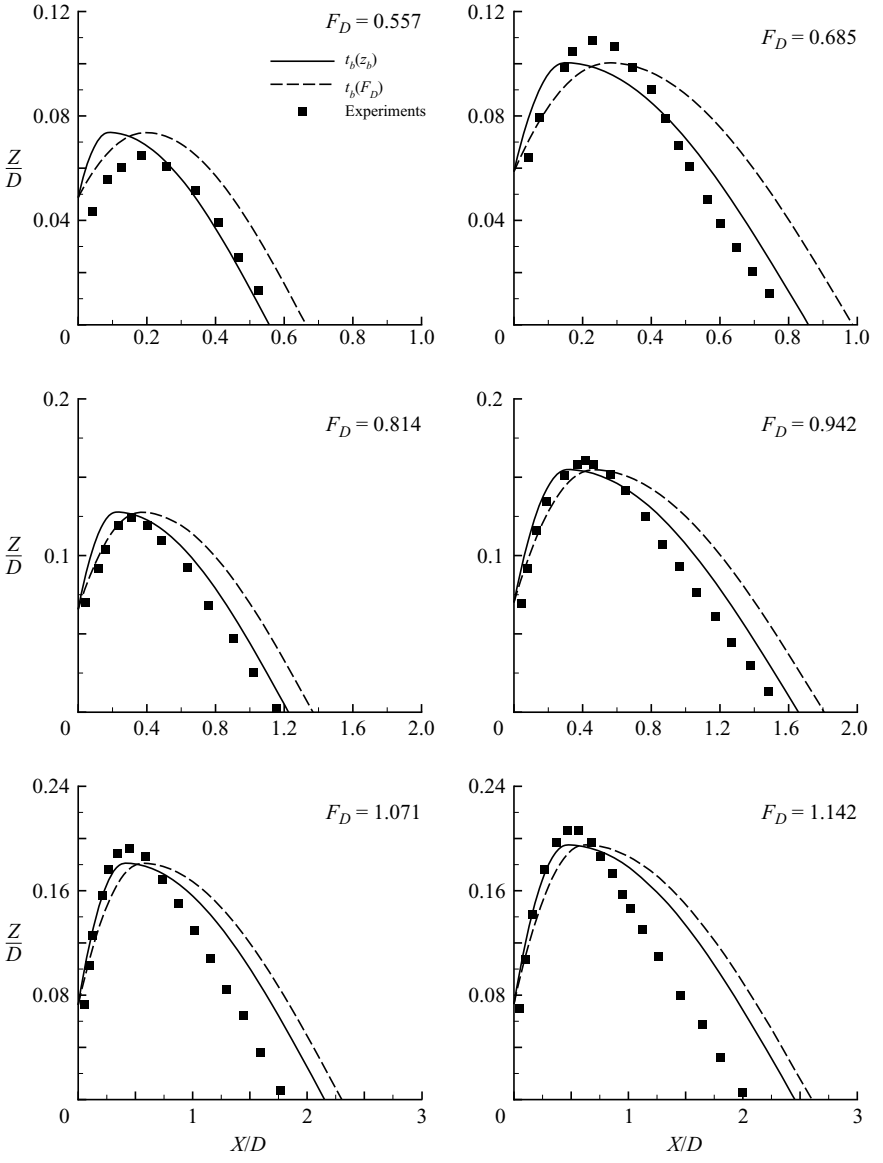

FIGURE 16. Theoretical bow wave profiles (11.1) and experimental measurements reported in Larrarte (1994) for a strut-like hull with entrance angle $2\alpha_E = 20°$. The draught-based Froude numbers F_D considered in this figure correspond to length-based Froude numbers equal to 0.203, 0.250, 0.297, 0.344, 0.391 and 0.417.

except for figure 21 for which no measurements were made for $\gamma = 15°$ (and for the highest speed $F_D = 1.784$, due to practical concerns about excessive hydrodynamic loads). Figures 17, 19 and 21 show that the wave profile is not overly affected by the heel angle γ for small values of γ, as assumed in the present study. The theoretical bow wave profiles in figures 15, 16, 18 and 20 are determined using the effective waterline entrance angle $\overline{\alpha_E}$ defined in Noblesse *et al.* (2006); similarly, the effective draught defined in Noblesse *et al.* (2006) is used for the theoretical wave profile of

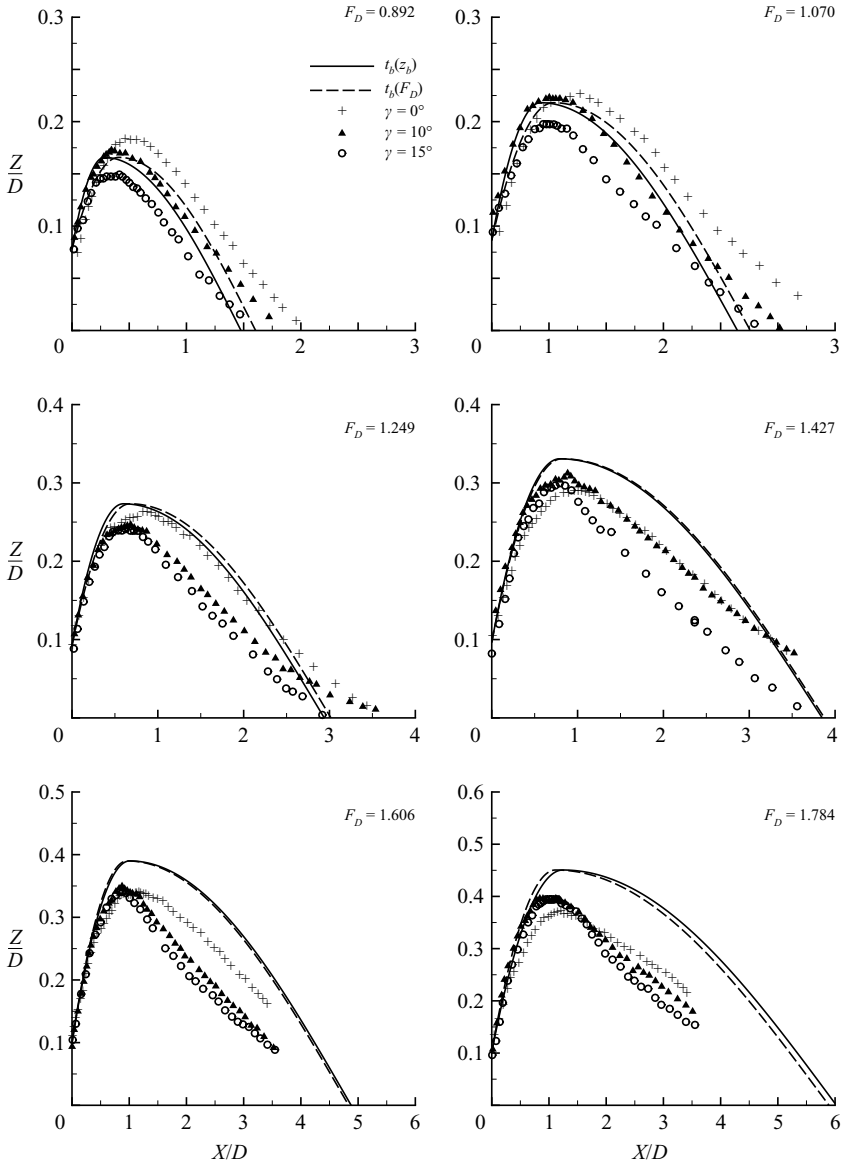

FIGURE 17. Theoretical bow wave profiles (11.1) and experimental measurements for a flat plate towed at a yaw angle $\alpha_E = 10°$ and heel angles $\gamma = 0°$, 10°, 15°. The draught-based Froude numbers F_D considered in this figure correspond to length-based Froude numbers equal to 0.451, 0.541, 0.632, 0.722, 0.812 and 0.902.

the Wigley hull in figure 15. However, the actual draught D is used for the horizontal and vertical coordinates X/D and Z/D in figures 15, 16, 18 and 20.

Experimental and theoretical bow wave profiles are compared for six values of the draught-based Froude number F_D for the Wigley hull (figure 15), the three Lararrte struts (figures 16, 18, 20), and the flat plate (figures 17, 19, 21). Figures 15 to 17 compare theoretical and experimental wave profiles for the Wigley hull, for which the waterline half-entrance angle α_E is approximately equal to 10°, the Lararrte 10° strut, and a flat plate towed at a yaw angle $\alpha_E = 10°$. Thus, these three figures correspond to

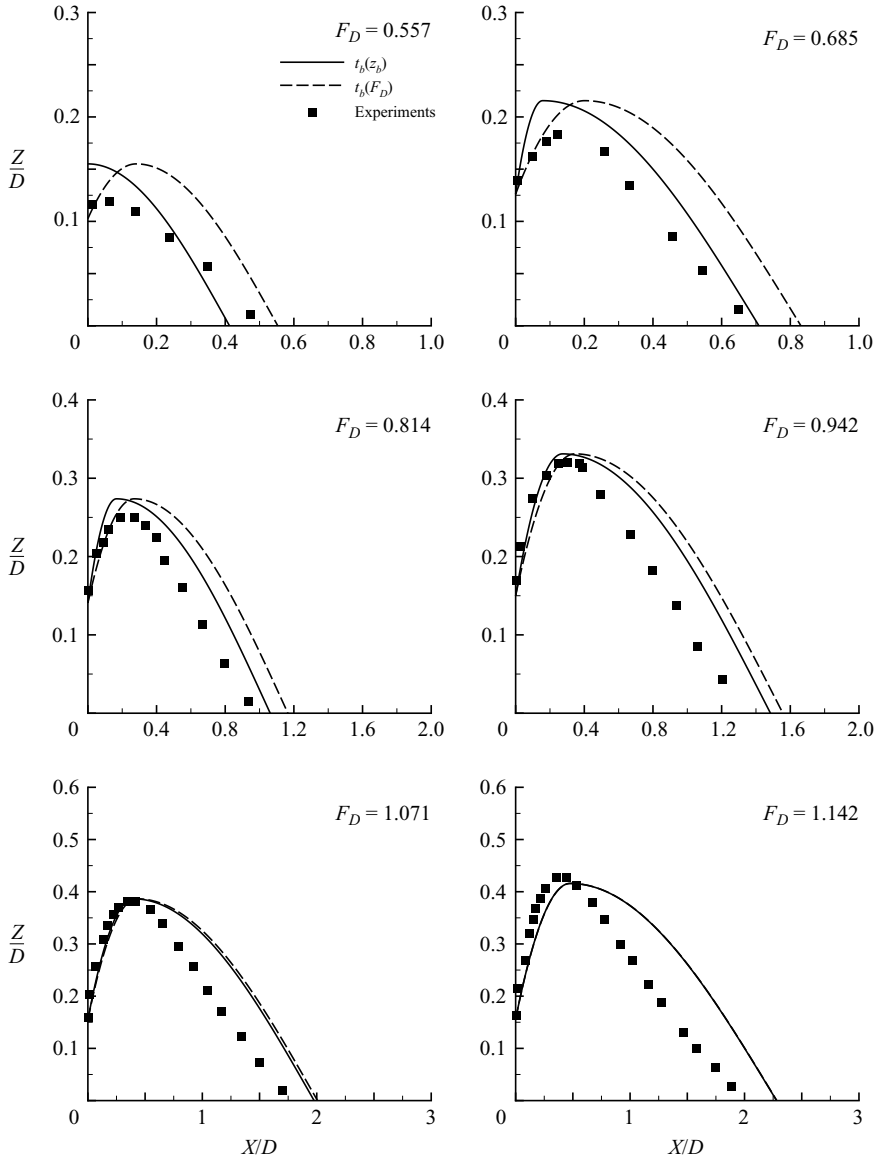

FIGURE 18. Theoretical bow wave profiles (11.1) and experimental measurements reported in Larrarte (1994) for a strut-like hull with entrance angle $2\alpha_E = 40°$.

the same waterline half-entrance angle $\alpha_E \approx 10°$. Figures 18, 19 and 20, 21 correspond to $\alpha_E = 20°$ and $\alpha_E = 30°$, respectively.

Differences between the theoretical wave profiles associated with the alternative expressions $t_b(z_b)$ and $t_b(F_D)$ given by (11.1*b*) depend on both the waterline half-entrance angle α_E and the Froude number F_D. These differences are relatively insignificant, and in fact are fairly small in figures 15, 17 and 19. The theoretical and experimental wave profiles in figures 15 to 17 are in reasonable agreement on the whole, especially at lower Froude numbers F_D. More precisely, the wavelength of the 'free-wave portion' of the theoretical profile (11.1*a*) becomes too large, in comparison to experimental measurements, for large values of F_D. These discrepancies appear to

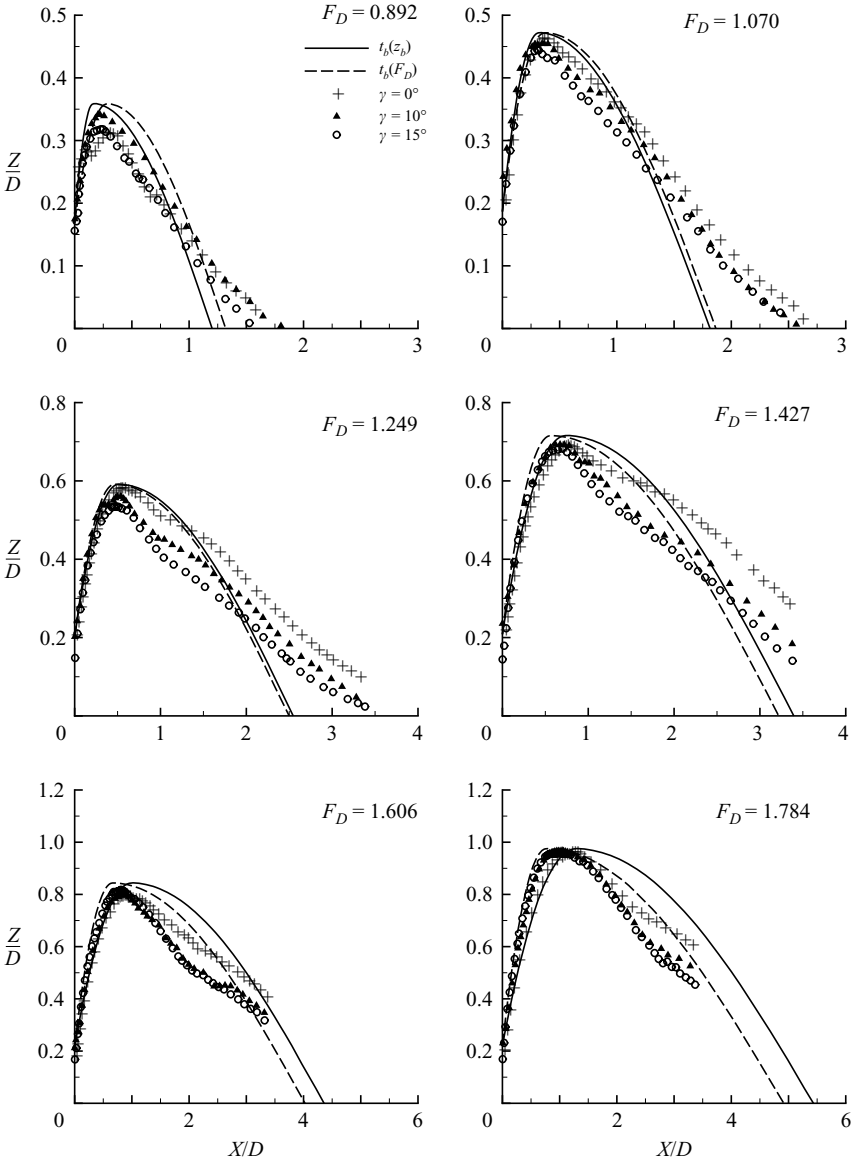

FIGURE 19. Theoretical bow wave profiles (11.1) and experimental measurements for a flat plate towed at a yaw angle $\alpha_E = 20°$ and heel angles $\gamma = 0°$, 10°, 15°.

be more pronounced in figures 15 and 16 than in figure 17. A possible explanation for these discrepancies is that the curvature of the Wigley hull and the Lararrte strut can be expected to have increasingly greater effects as the speed U and the wavelength $2\pi(\cos^2\alpha_E)U^2/g$ increase. The amplitude of the bow wave is fairly well predicted on the whole, especially for the Wigley hull (figure 15) and the Lararrte strut (figure 16). Agreement between theoretical and experimental wave profiles does not appear to be worse in figures 18 and 19, which correspond to $\alpha_E = 20°$, than in figures 15 to 17 for $\alpha_E = 10°$. In fact, theoretical profiles are in better agreement with experimental measurements for the flat plate held at a yaw angle $\alpha_E = 20°$ (figure 19) than at the smaller angle $\alpha_E = 10°$ (figure 17). Similarly, theoretical profiles, especially the

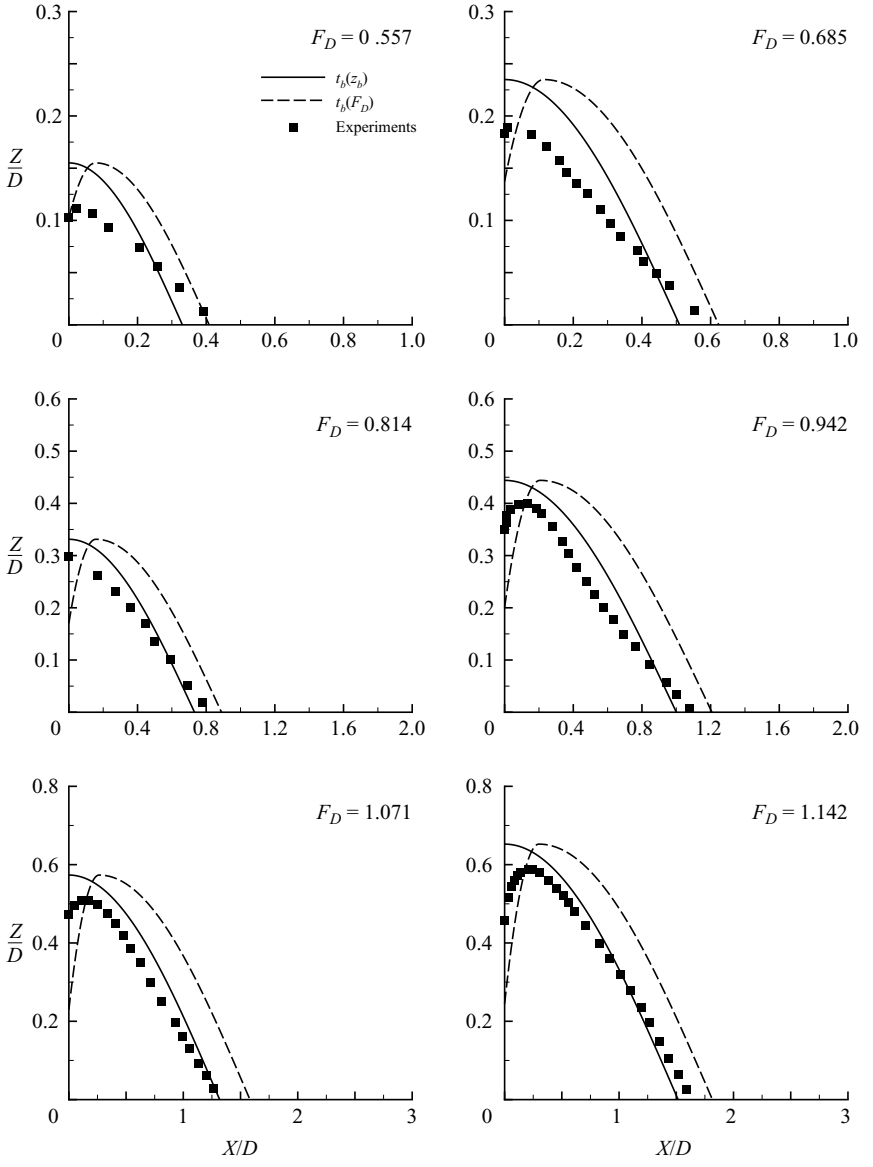

FIGURE 20. Theoretical bow wave profiles (11.1) and experimental measurements reported in Larrarte (1994) for a strut-like hull with entrance angle $2\alpha_E = 60^\circ$.

$t_b(z_b)$ profiles, agree fairly well with experimental measurements in figure 20, which corresponds to the Lararrte strut with a large waterline entrance angle $2\alpha_E = 60^\circ$ (for which the bow wave is unsteady). However, agreement between theoretical and experimental wave profiles is poor (except for the wave amplitude, which is fairly well predicted) in figure 21 for the flat plate towed at a yaw angle $\alpha_E = 30^\circ$. Figures 20 and 21 show that free-surface flows about a flat plate towed at a yaw angle α_E and a ship hull with a wedge-like bow and waterline entrance angle $2\alpha_E$ differ significantly for large values of α_E, as one might expect (and in accordance with our flow observations).

In summary, figures 15 to 20 show that, in spite of its great simplicity, the analytical approximation to a ship bow wave profile given by (11.1) and (8.2)

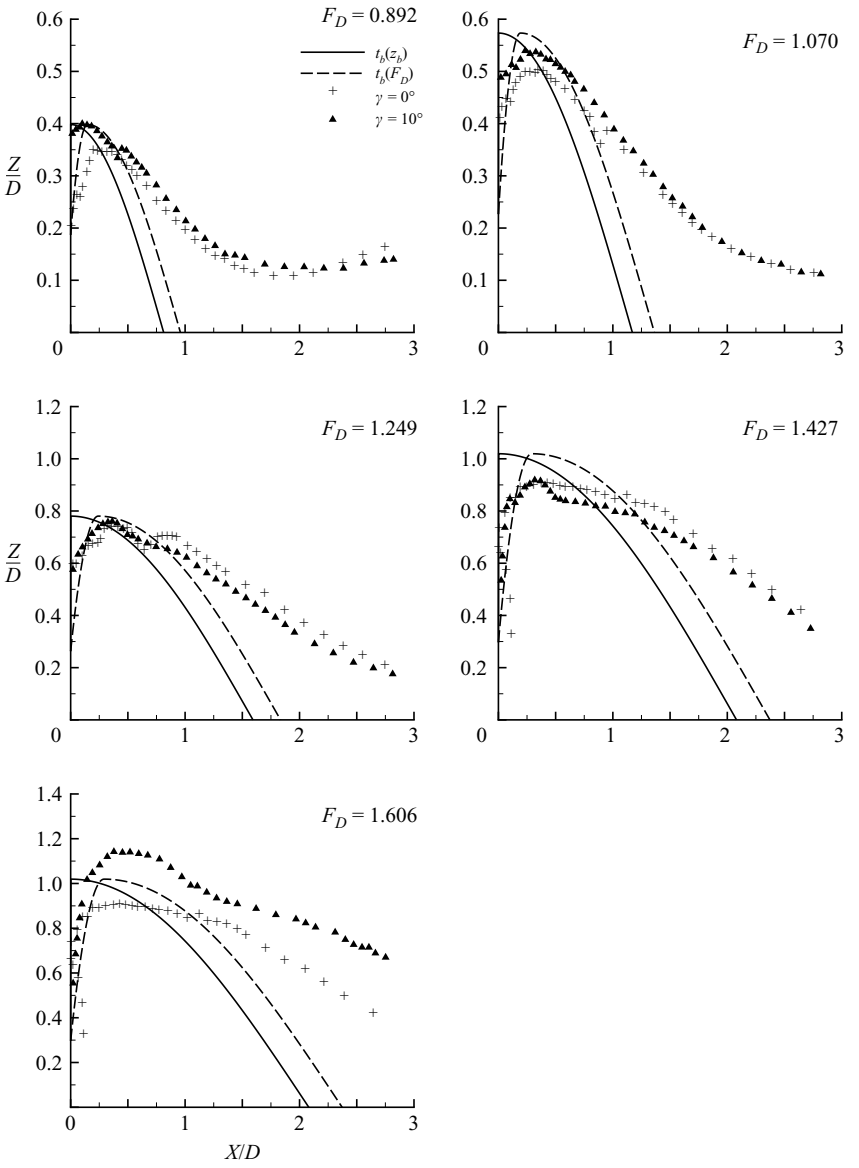

FIGURE 21. Theoretical bow wave profiles (11.1) and experimental measurements for a flat plate towed at a yaw angle $\alpha_E = 30°$ and heel angles $\gamma = 0°$ and $10°$.

is in reasonable agreement with experimental measurements. In particular, this approximation correctly predicts the variations of a ship bow wave profile associated with variations of the ship speed U, draught D, and waterline entrance angle $2\alpha_E$; a property that is of considerable importance for practical applications to ship design.

13. Conclusion

In summary, the bow wave generated by a ship – that has a non-bulbous wedge-shaped bow with small flare angle – in steady motion has been considered using experimental measurements and elementary fundamental considerations (dimensional

analysis, rudimentary asymptotic considerations in the thin-ship, shallow-draught and deep-draught limits, thin-ship theory, elementary Lagrangian analysis based on Newton's equations for a single water particle, and elementary wave). This elementary analysis has led to a series of simple relations that define essential features of a ship bow wave, directly and without calculations, in terms of the ship speed U, draught D, and waterline entrance angle $2\alpha_E$.

Specifically, a simple criterion that determines whether a ship in steady motion can be expected to generate a 'steady' overturning bow wave or an unsteady wave has been given. Simple expressions for the height of a ship bow wave, the distance between the stem and the bow wave crest of a ship, the rise of water at a ship stem, and the shape of the bow wave (bow wave profile) have also been given. In spite of their remarkable simplicity, these relations are in reasonable agreement with experimental measurements and observations both for several hulls with non-bulbous wedge-shaped bows and for a rectangular flat plate towed at a yaw angle α_E.

The simple expressions given in the study provide explicit relationships between main characteristics of a ship bow wave (wave height, location and profile; flow steadiness or unsteadiness) and basic 'design parameters' (ship speed, draught, waterline entrance angle). In other words, these expressions provide direct 'cause-and-effect' relations between basic design parameters and essential bow wave features. Such direct relations provide valuable insight, and are sufficiently accurate to be useful for practical applications to ship design, notably at early design stages (concept and preliminary design).

The work of the first author was sponsored by NSWCCD's ILIR research program and the Naval Surface Warfare Center Carderock Division (NSWCCD) in support of the Naval Sea Systems Command's Joint High Speed Sealift (JHSS) program. Mr John Offutt, JHSS Technology Manager, was the technical monitor.

REFERENCES

Brard, R. 1972 The representation of a given ship form by singularity distributions when the boundary condition on the free surface is linearized. *J. Ship Res.* **16**, 79–92.

Bulgarelli, U. P. 2005 The application of numerical methods for the solution of some problems in free-surface hydrodynamics. *J. Ship Res.* **49**, 288–301.

Çalışal, S. M. & Chan, J. L. K. 1989 A numerical modeling of ship bow waves. *J. Ship Res.* **33**, 21–28.

Chapman, R. B. 1976 Free surface effects for yawed surface-piercing plate. *J. Ship Res.* **20**, 125–136.

Dawson, C. W. 1977 A practical computer method for solving ship-wave problems. In *Second Intl Conf. on Numerical Ship Hydrodynamics, Berkeley, CA*, pp. 30–38.

Dong, R. R., Katz, J. & Huang, T. T. 1997 On the structure of bow waves on a ship model. *J. Fluid Mech.* **346**, 77–115.

Farmer, J., Martinelli, L. & Jameson, A. 1993 A fast multigrid method for solving the nonlinear ship wave problem with a free surface. In *Sixth Intl Conf. on Numerical Ship Hydrodynamics, Iowa City, IA*.

Fontaine, E., Faltinsen, O. M. & Cointe, R. 2000 New insight into the generation of ship bow waves. *J. Fluid Mech.* **321**, 15–38.

Hino, T. 1997 An unstructured grid method for incompressible viscous flows with a free surface. *AIAA Paper* 97-0862.

Jensen, G., Bertram, V. & Söding, H. 1989 Ship wave-resistance computations. In *Fifth Intl Conf. on Numerical Ship Hydrodynamics, Hiroshima, Japan*, pp. 593–606.

Kajitani, H., Miyata, H., Ikehata, M., Tanaka, H., Adachi, H., Namimatsu, M. & Ogiwara, S. 1983 *Second DTNSRDC Workshop on Ship Wave-Resistance Computations.* David Taylor Naval Ship Research and Development Center, MD USA.

Karion, A., Sur, T. W., Fu, T. C., Furey, D. A., Rice, J. R. & Walker, D. C. 2003 Experimental study of the bow wave of a large towed wedge. In *Eighth Intl Conf. on Numerical Ship Hydrodynamics, Busan, Korea.*

Landrini, M. 2006 Strongly nonlinear phenomena in ship hydrodynamics. *J. Ship Res.* **50**, 99–119.

Larrarte, F. 1994 Étude expérimentale et théorique des profils de vagues le long d'une carène. Thèse de doctorat, Univ. de Nantes et École Centrale de Nantes.

McCarthy, J. H. 1985 Collected experimental resistance component and flow data for three surface ship model hulls. *David W. Taylor Naval Ship Research and Development Center*, Rep. DTNSRDC-85/011.

Maniar, H., Newman, J. N. & Xu, H. 1991 Free-surface effects on a yawed surface-piercing plate. *Eighteenth Symp. on Naval Hydrodynamics* 273–283. National Academy Press.

Muscari, R. & Di Mascio, A. 2004 Numerical modelling of breaking waves generated by a ship's hull. *J. Mar. Sci. Tech.* **9**, 158–170.

Noblesse, F. 1983 A slender-ship theory of wave resistance. *J. Ship Res.* **27**, 13–33.

Noblesse, F. & Dagan, G. 1976 Nonlinear ship-wave theories by continuous mapping. *J. Fluid Mech.* **75**, 347–371.

Noblesse, F., Hendrix, D., Faul, L. & Slutsky, J. 2006 Simple analytical expressions for the height, location, and steepness of a ship bow wave. *J. Ship Res.* **50**, 360–370.

Noblesse, F., Delhommeau, G., Guilbaud, M. & Yang, C. 2008 The rise of water at a ship stem. *J. Ship Res.*, in press.

Ogilvie, T. F. 1967 Nonlinear high-Froude number free-surface problems. *J. Engng Maths* **1**, 215–235.

Ogilvie, T. F. 1973 The wave generated by a fine ship bow. *Ninth Intl Symp. on Naval Hydrodynamics* pp. 1483–1524. National Academy Press.

Queutey, P. & Visonneau, M. 2007 An interface capturing method for free-surface hydrodynamic flows. *Computers Fluids* **36**, 1481–1510.

Raven H. C. 1999 Inviscid calculations of ship wave making capabilities, limitations, and prospects. *Twenty-Second Symp. on Naval Hydrodynamics* pp. 27–42. National Academy Press.

Roth, G. I. Mascenik, D. T. & Katz, J. 1999 Measurements of the flow structure and turbulence within a ship bow wave. *Phys. Fluids*, **11**, 3512–3523.

Scragg, C. A. & Talcott, J. 1991 Numerical solution of the Dawson free-surface problem using Havelock singularities. *Eighteenth Symp. on Naval Hydrodynamics*, pp. 259–283. National Academy Press.

Standing, R. G. 1974 Phase and amplitude discrepancies in the surface wave due to a wedge-ended hull form. *J. Fluid Mech.* **62**, 625–642.

Subramani, A., Beck, R. & Scorpio, S. 1999 Fully nonlinear free-surface computations for arbitrary and complex hull forms. *Twenty-Second Symp. on Naval Hydrodynamics*, pp. 47–58. National Academy Press.

Tuck, E. O. 1966 Shallow-water flows past slender bodies. *J. Fluid Mech.* **26**, 81–95.

Tulin, M. P. & Landrini, M. 2001 Breaking waves in the ocean and around ships. *Twenty Third Symp. on Naval Hydrodynamics.* National Academy Press.

Waniewski, T. A., Brennen, C. E. & Raichlen, F. 2002 Bow wave dynamics. *J. Ship Res.* **46**, 1–15.

Wilson, R. V., Carrica, P. M. & Stern, F. 2006 URANS simulations for a high-speed transom stern ship with breaking waves. *Intl J. Comput. Fluid Dyn.* **20**, 105–125.

Wyatt, D. C. 2000 Development and assessment of a nonlinear wave prediction methodology for surface vessels. *J. Ship Res.* **44**, 96–107.

Xu, H. 1991 A potential flow solution for a yawed surface-piercing plate. *J. Fluid Mech.* **226**, 291–317.

Yang, C. & Löhner, R. 2002 Calculation of ship sinkage and trim using a finite element method and unstructured grids. *Intl J. Comput. Fluid Dyn.* **16**, 217–227.